



Direct Contact Membrane Distillation for Water Reuse Using Nanostructured Ceramic Membranes

WaterReuse Research Foundation

Direct Contact Membrane Distillation for Water Reuse Using Nanostructured Ceramic Membranes

About the WaterReuse Research Foundation

The mission of the WaterReuse Research Foundation is to conduct and promote applied research on the reclamation, recycling, reuse, and desalination of water. The Foundation's research advances the science of water reuse and supports communities across the United States and abroad in their efforts to create new sources of high-quality water through reclamation, recycling, reuse, and desalination while protecting public health and the environment.

The Foundation sponsors research on all aspects of water reuse, including emerging chemical contaminants, microbiological agents, treatment technologies, salinity management and desalination, public perception and acceptance, economics, and marketing. The Foundation's research informs the public of the safety of reclaimed water and provides water professionals with the tools and knowledge to meet their commitment of increasing reliability and quality.

The Foundation's funding partners include the Bureau of Reclamation, the California State Water Resources Control Board, the California Energy Commission, and the California Department of Water Resources. Funding is also provided by the Foundation's Subscribers, water and wastewater agencies, and other interested organizations.

Direct Contact Membrane Distillation for Water Reuse Using Nanostructured Ceramic Membranes

Mark Wiesner, Ph.D.
Duke University

Zachary Hendren, Ph.D.
Duke University

Cosponsor

Bureau of Reclamation



WaterReuse Research Foundation
Alexandria, VA



Disclaimer

This report was sponsored by the WateReuse Research Foundation and cosponsored by the Bureau of Reclamation. The Foundation, its Board Members, and the project cosponsors assume no responsibility for the content of this publication or for the opinions or statements of facts expressed in the report. The mention of trade names of commercial products does not represent or imply the approval or endorsement of the WateReuse Research Foundation, its Board Members, or the cosponsors. This report is published solely for informational purposes.

For more information, contact:

WateReuse Research Foundation
1199 North Fairfax Street, Suite 410
Alexandria, VA 22314
703-548-0880
703-548-5085 (fax)
www.WateReuse.org/Foundation

© Copyright 2013 by the WateReuse Research Foundation. All rights reserved. Permission to reproduce must be obtained from the WateReuse Research Foundation.

WateReuse Research Foundation Project Number: WRF-07-05
WateReuse Research Foundation Product Number: 07-05-1

ISBN: 978-1-934183-86-1

Contents

List of Figures	vii
List of Tables	ix
List of Acronyms	x
List of Symbols	xi
Foreword	xiii
Acknowledgments	xiv
Executive Summary	xv
Chapter 1. Introduction	1
1.1 Project Objectives	1
1.2 Membrane Distillation Background and Energetic Considerations	2
1.3 Modeling the Heat and Mass Transfer in Membrane Distillation	2
1.4 Temperature Polarization	5
1.5 Membrane Distillation/Reverse Osmosis Energy Comparison	5
Chapter 2. Ceramic Membrane Surface Modification	9
2.1 Membrane Materials for Membrane Distillation	9
2.2 Ceramic Surface Modification	10
2.3 Hydrophobic Solution Grafting	10
2.4 Membrane Characterization	12
2.5 LEP Measurement	12
2.6 TCS vs. PFS Membrane Surface Coating	13
2.7 Membrane Durability	15
2.8 Ceramic Membrane Tensile Strength	15
2.9 Membrane Resistance to Chlorine	18
2.10 Membrane Performance Comparison	19
2.11 Membrane Distillation Module	19
2.12 Model Validation and Ceramic/Polymeric Performance Comparison	19
Chapter 3. Organic Matter Fouling in Membrane Distillation	23
3.1 Fouling in Membrane Distillation	23
3.2 Synthetic Foulants	24
3.3 Selection and Characterization of Model Foulants	24
3.4 Size and Zeta Potential Measurements	25
3.5 Membrane Distillation Fouling Studies using Model Foulants	28
3.6 Synthetic Fouling Studies	28
3.7 Synthetic Foulant Effect on LEP	34

3.8 Membrane Distillation of 2 ^o Clarified Effluent.....	36
3.9 b Wastewater Fouling Tests	36
3.10 Membrane-Cleaning Experiments.....	38
3.11 Wastewater Fouling Effect on LEP.....	42
Chapter 4. Conclusions and Final Recommendations	43
References	45

Figures

1.1	Representative view of the MD process where water is transported in vapor form from the feed to the condensing solution.....	2
1.2	Schematic showing the temperature distribution during DCMD and countercurrent flow.....	3
1.3	Flux as a function of ionic strength for hypothetical RO and MD modules.....	6
1.4	Cost comparison between RO and MD technologies assuming energy consumption at midpoint of 44.5 kWh/m ³ and two different heat sources.....	7
2.1	Contact angle measurement of anodisc membrane (a) before and (b) after PFS grafting	11
2.2	FTIR absorbance spectra of 200-nm alumina anodisc membranes with surface treatments of (a) PFS and (b) TCS. The FTIR spectra for an unmodified anodisc membrane are included in each figure for comparison.. ..	11
2.3	Representative SEM images of (a) an unmodified anodisc membrane and after coating with (b) PFS and (c) TCS grafting solutions	12
2.4	Schematic of LEP measurement for a disc membrane. The LEP is the pressure indicated on the gauge when the first drop of water permeates through the membrane.	13
2.5	Representative SEM images of (a) an unmodified anodisc and (b) a TF-200 membrane surface. Both membranes have a reported mean pore diameter of 200 nm.....	15
2.6	Stress–strain curves for unmodified and PFS-treated anodisc membranes exposed to different drying times	16
2.7	Angle of contact with water as a function of exposure time to a 2.82 mM free chlorine solution at three different pHs for (a) a PFS-treated anodisc membrane, (b) a TCS-treated anodisc membrane, and (c) a TF-200 membrane (T = 20 °C, n = 3)	17
2.8	Schematic showing the DCMD bench-scale test unit used in this investigation.....	19
2.9	Water flux across (a) PFS anodisc and (b) TF-200 membranes during DCMD of DI water as a function of feed/permeate temperature difference	20
3.1	Representative intensity-weighted particle size distributions of (a) sodium alginate, (b) humic acid, and (c) CML colloids in 0.01 M CaCl ₂ solutions at different pH values	26
3.2	Relative flux as a function of time for MD tests of synthetic organic foulants at a concentration of 50 mg/L for anodisc membrane coupons filtering water over 24 h at (a) pH=3, (b) pH=7, and (c) pH=10.. ..	29
3.3	Relative flux as a function of time for MD tests of synthetic organic foulants at a concentration of 50 mg/L for TF-200 membrane coupons filtering water over 24 h at (a) pH=3, (b) pH=7, and (c) pH=10.....	30

3.4	Representative SEM images of fouled membranes: (a) TF-200, humic acid, pH=7, (b) anodisc, CML, pH=10, (c) anodisc, alginate, pH=7, (d) TF-200, alginate, pH=3, (e) TF-200, BSA, pH=3, and (f) anodisc, BSA, pH=7.....	31
3.5	LEP results for PTFE membranes fouled with synthetic foulants averaged for all three pH values.	35
3.6	LEP results for PFS anodisc membranes fouled with synthetic foulants averaged for all three pH values	35
3.7	Relative flux as a function of time for TF-200 and PFS membranes during MD of 2° clarified effluent from the North Durham Water Reclamation Facility.....	37
3.8	Membrane distillation of secondary clarified wastewater incorporating one of three cleaning solutions. PFS anodisc membranes... ..	39
3.9	Membrane distillation of secondary clarified wastewater incorporating one of three cleaning solutions. TF-200 membranes	39
3.10	Representative images of membranes after filtering wastewater via MD before and after cleaning: (a) fouled TF-200 membrane, (b) fouled PFS membrane, (c) TF-200 membrane cleaned with NaOCl at pH=7, (d) PFS membrane cleaned with NaOCl at pH=10, (e) TF-200 membrane cleaned with NaOCl at pH=10, and (f) PFS membrane cleaned with DI water.	41
3.11	LEP results for PFS anodisc and TF-200 membranes fouled with secondary clarified effluent from the North Durham Water Reclamation Facility.....	42

Tables

1.1	Desalination Technology Energy Comparison.....	6
2.1	Summary of Water Fluxes Measured by Previous Researchers Investigating Direct Contact Membrane Distillation and Vacuum-Enhanced Membrane Distillation.....	9
2.2	Measured and Calculated Values of the TF-200 and Anodisc Membranes Modified Using PFS and TCS.....	14
2.3	Theoretical Flux for PFS 200-nm Anodisc Membranes Calculated Incorporating Physical Characteristics from the TF-200 Membranes Used in This Study.....	21
3.1	Summary of Size and Zeta Potential Measurements for the NOM Suspensions To Be Used During Fouling Experiments.....	27
3.2	Final Relative Flux Value for Each Synthetic Fouling Experimental Test, Averaged by Foulant Type and by pH. PFS Anodisc Tests.....	33
3.3	Final Relative Flux Value for Each Synthetic Fouling Experimental Test, Averaged by Foulant Type and by pH. TF-200 Tests.....	33
3.4	NPDES Permit Limits and Average Monthly Discharge Values for the North Durham Water Reclamation Facility.....	36
3.5	Measured Values of Key Discharge Parameters for Secondary Clarified Wastewater Filtered Via MD with Both PFS and PTFE Membranes.....	38

Acronyms

AFM	atomic force microscopy
BET	Brunauer-Emmett-Teller
CML	carboxylate modified latex
DCMD	direct contact membrane distillation
DDW	doubly deionized water
DI	deionized
EPS	extracellular polymeric substances
FTIR	Fourier transform infrared
HCl	hydrochloric acid
LEP	liquid entry pressure
MD	membrane distillation
MF	microfiltration
MSF	multistage flash distillation
NaOCl	sodium hypochlorite
NaOH	sodium hydroxide
NF	nanofiltration
NOM	natural organic matter
NPDES	National Pollutant Discharge Elimination System
PFS	perfluorodecyltriethoxysilane
PTFE	polytetrafluoroethylene
PVDF	polyvinylidene difluoride
RO	reverse osmosis
SEM	scanning electron microscopy
TCS	trichloromethylsilane
TMS	trimethylchlorosilane
TMP	transmembrane pressure
TPC	temperature polarization coefficient
UF	ultrafiltration

Symbols

Symbol	Description	Representative Unit
D_{Kn}	Knudsen diffusion	m^2/s
D_m	molecular diffusion	m^2/s
f	feed side of membrane	N/A
h	heat transfer coefficient	W/m^2-K
H_v	water latent heat of vaporization	J/kg
J	water flux across membrane	kg/m^2-h
k_B	Boltzmann constant	J/K
l_i	molecular mean free path	m
m	membrane	N/A
M_w	molecular weight	g/mol
Nu	Nusselt number	N/A
p	permeate side of membrane	N/A
P	vapor pressure	Pa
q	specific heat flux	W/m^2
R	gas constant	J/mol-K
T	temperature	K
U	overall heat transfer coefficient	W/m^2-K
χ	tortuosity	N/A
δ	thickness	m
ε	porosity	N/A
λ	thermal conductivity	W/m-K

Foreword

The WaterReuse Research Foundation, a nonprofit corporation, sponsors research that advances the science of water reclamation, recycling, reuse, and desalination. The Foundation funds projects that meet the water reuse and desalination research needs of water and wastewater agencies and the public. The goal of the Foundation's research is to ensure that water reuse and desalination projects provide high-quality water, protect public health, and improve the environment.

An Operating Plan guides the Foundation's research program. Under the plan, a research agenda of high-priority topics is maintained. The agenda is developed in cooperation with the water reuse and desalination communities including water professionals, academics, and Foundation subscribers. The Foundation's research focuses on a broad range of water reuse research topics including:

- Definition of and addressing emerging contaminants
- Public perceptions of the benefits and risks of water reuse
- Management practices related to indirect potable reuse
- Groundwater recharge and aquifer storage and recovery
- Evaluation and methods for managing salinity and desalination
- Economics and marketing of water reuse

The Operating Plan outlines the role of the Foundation's Research Advisory Committee (RAC), Project Advisory Committees (PACs), and Foundation staff. The RAC sets priorities, recommends projects for funding, and provides advice and recommendations on the Foundation's research agenda and other related efforts. PACs are convened for each project and provide technical review and oversight. The Foundation's RAC and PACs consist of experts in their fields and provide the Foundation with an independent review, which ensures the credibility of the Foundation's research results. The Foundation's Project Managers facilitate the efforts of the RAC and PACs and provide overall management of projects.

The objectives of this project were to (a) develop and characterize ceramic membranes to have the necessary chemical and physical properties for use in direct contact membrane distillation (DCMD), (b) integrate these membranes into a laboratory-scale unit, and (c) evaluate the performance of these membranes alongside a polytetrafluoroethylene polymeric counterpart during treatment of different synthetic solutions containing organic foulants as well as wastewater from the North Durham Water Reclamation Facility. The project is intended to inform the water reuse community on the benefits and tradeoffs of using ceramic membranes in DCMD as well as provide performance information on membrane distillation as an advanced treatment technology.

Richard Nagel
Chair
WaterReuse Research Foundation

G. Wade Miller
Executive Director
WaterReuse Research Foundation

Acknowledgments

This project was funded by the WateReuse Research Foundation in cooperation with the Bureau of Reclamation, Duke University, and the City of Durham–Wastewater Division.

The research team expresses its gratitude toward a number of people who helped make this study possible. They include the members of the research team and PAC members (as identified in the following) and the WateReuse Research Foundation’s project manager, Anna Durden, as well as John Dodson and the entire operation staff at the North Durham Water Reclamation Facility (WRF).

The research team thanks the WateReuse Research Foundation and the U.S. Bureau of Reclamation for funding this applied research project, as well as the North Durham WRF for its in-kind contributions.

Principal Investigator and Project Manager

Mark R. Wiesner, Ph.D., *Duke University*

Research Project Team

John Dodson and colleagues, *North Durham Water Reclamation Facility*

Soryong Chae, *The University of Sydney*

Zachary Hendren, *Duke University*

Project Advisory Committee

Katherine Guerra, *Bureau of Reclamation*

Jonathan Brant, *University of Wyoming*

Amy Childress, *University of Nevada*

Shankar Chellam, *University of Houston*

Executive Summary

This research report increases our knowledge base on a technology that holds significant promise for water reuse—membrane distillation (MD). The objectives of this project were to (a) develop and characterize ceramic membranes to have the necessary chemical and physical properties for use in direct contact MD (DCMD), (b) integrate these membranes into a laboratory-scale unit, and (c) evaluate the performance of these membranes alongside a polytetrafluoroethylene (PTFE) polymeric counterpart during treatment of different synthetic solutions containing organic foulants as well as wastewater from the North Durham Water Reclamation Facility. The project is intended to inform the water reuse community on the benefits and tradeoffs of using ceramic membranes in DCMD as well as to provide performance information on MD as an advanced treatment technology.

The ceramic membranes were successfully modified by using chemical surface treatments to possess the necessary hydrophobic characteristics for operation in DCMD. In addition, these modified membranes were shown to exhibit the physical, thermal, and chemical characteristics that would allow operation/cleaning under harsh conditions that would exceed the limitations of the PTFE membrane. Both membrane types tested demonstrated the following:

1. They maintained the necessary hydrophobicity to operate after exposure to the following domestic wastewater and organic foulants: alginate, humic acid, bovine serum, and latex particles. The foulants remained on the membrane surface rather than entering the pore matrix, which prevented the occurrence of pore flooding that would damage the membrane integrity.
2. The effluent quality from both membranes was of high quality, easily exceeding permitting standards, and from that aspect MD poses a low risk to utilities for implementation.
3. Virtually complete flux recovery of membranes fouled during filtration of wastewater (both ceramic and polymeric) occurred when a chlorinated treatment solution was used as well as plain deionized (DI) water.

Finally, membrane performance was evaluated during the treatment of water containing various specific organic foulants and during the treatment of municipal wastewater. The results showed that the level of fouling was highly dependent on foulant type, with alginate identified as a component that produces severe fouling under all conditions evaluated (and for both membrane types) and with wastewater fouling being relatively minimal. Given the limited time frame of the fouling experiments (24 h), additional long-term testing is necessary to fully evaluate the effects of increased exposure to foulants on MD performance. Fouling is still likely to be a major problem at scale-up because many potential applications involving MD will be for the treatment of high-concentration water.

It is our belief that the information provided contributes to the growing information base on MD technology, which we hope spurs further research to develop this promising water treatment alternative on the pilot scale. This development should prove to be of interest to both researchers and prospective users, as the production of high-quality effluent for minimal energy input is a potential game-changer in water reuse applications.

Chapter 1

Introduction

1.1 Project Objectives

In contrast with pressure-driven membrane processes such as reverse osmosis (RO), nanofiltration (NF), ultrafiltration (UF), and microfiltration (MF), membrane distillation (MD) is a desalting process that is driven by a thermal gradient. A particularly exciting application of MD is in the area of water reuse through the advanced treatment of wastewater or desalination of waste brines where diffuse heat can be tapped as the driving force for membrane separation. In addition to the ability to use diffuse heat as a driving force, MD offers several advantages over RO or NF as a desalting process.

Inherent to the pressure-driven process is a buildup of osmotic pressure, $\Delta\pi$, which makes increasing water recovery by increasing the energy input to produce clean water uneconomical, which in turn causes precipitative fouling as the feed concentration increases. As a result, RO is typically limited to recoveries of 40–70% of the feed, the lowest being for the RO treatment of high-salinity seawater^[1, 2]. One advantage of MD as a treatment option is that a temperature gradient rather than a pressure gradient serves as the driving force for transport, which diminishes the effect of osmotic back pressure as a barrier to water recovery. In the direct contact MD (DCMD) configuration, a warm feed stream is allowed to flow on one side of a membrane, whereas a colder permeate, or condensing stream, flows on the opposite side. The vapor pressure differential results in evaporation of water from the warm side and condensation on the cold side (Figure 1.1). Because only water is being transferred in the absence of volatile solutes in the feed, the resulting product water is of very high purity [3, 4]. In addition to being an attractive alternative to RO, MD may also be useful as a process for treating RO concentrate.

The application of MD in the context of water reclamation or concentrate treatment will require an extremely robust membrane. These MD membranes must withstand rigorous chemical cleaning and the physical stresses imposed by backflushing to remove foulants that are likely to be present in the feed water in such applications. Ceramic membranes are excellent candidates in this regard. This work details the modification and implementation of aluminum oxide nanostructured ceramic membranes in a working bench-scale DCMD process. The modified membranes are thoroughly characterized, and their performance in treating various organic foulant-laden waters is evaluated alongside a polytetrafluoroethylene (PTFE) counterpart. Their performance in treating actual wastewater from the North Durham Water Reclamation Facility is also examined in parallel studies. The following research objectives were identified:

1. Develop and characterize ceramic membranes that possess the structural stability, pore size distribution, hydrophobicity, and modified surface chemistries for use in DCMD.
2. Integrate these membranes into a bench-scale unit.
3. Evaluate the performance of these membranes for water reuse applications at bench scale in conditions representing wastewater and with actual wastewater.

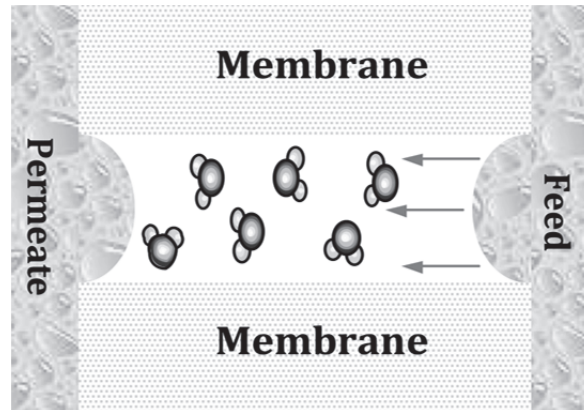


Figure 1.1. Representative view of the MD process where water is transported in vapor form from the feed to the permeate solution.

1.2 Membrane Distillation Background and Energetic Considerations

A number of energetic inefficiencies have been identified in MD processes, which include temperature polarization [5-7]; resistance to vapor flow through the membrane, which is a function of membrane characteristics such as porosity, interfacial energy, and pore structure [8]; and conductive heat loss through the membrane [9]. Each of these inefficiencies may be addressed through improved and innovative membrane design and the use of nonpolymeric materials like ceramics. For instance, Cath et al. [5] pointed out that polymeric materials have reached their design limits in terms of porosity and similarities in heat conductivities.

1.3 Modeling the Heat and Mass Transfer in Membrane Distillation

Because the heat and mass transfer are dependent on one another, they must each be evaluated separately and simultaneously. Although equations describing the heat transfer in MD are readily available [10-14], a brief summary is provided for a general case of DCMD as depicted in Figure 1.2.

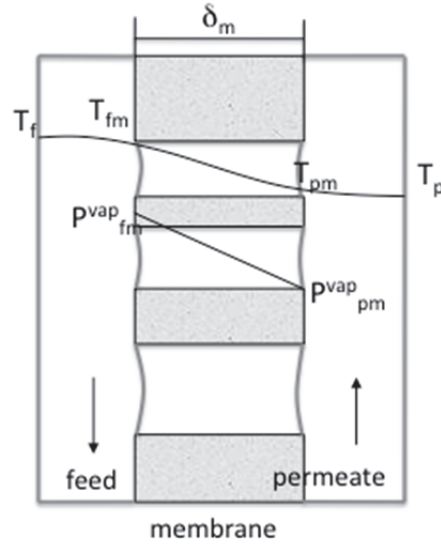


Figure 1.2. Schematic showing the temperature distribution during DCMD and countercurrent flow.

In DCMD, heat transfer occurs in three steps, through the feed-side boundary layer, the membrane itself, and the permeate-side boundary layer, which can be represented as

$$q_f = h_f (T_f - T_{fm}) \quad (1)$$

$$q_m = JH_v + \lambda_m \frac{(T_{fm} - T_{pm})}{\delta_m} \quad (2)$$

$$q_p = h_p (T_{pm} - T_p) \quad (3)$$

where h is the heat transfer coefficient, q is the heat flux, λ is the thermal conductivity, J is the water flux, δ is the membrane thickness, and H_v is the heat of vaporization of water. For the equivalent thermal circuit of the membrane and the boundary layers, the three associated resistances are $R_1 = (T_f - T_{fm})/q_f$, $R_2 = (T_{fm} - T_{pm})/q_m$, and $R_3 = (T_{pm} - T_p)/q_p$, which are combined to determine the overall heat transfer coefficient for the equation $Q_{tot} = U\Delta T$, where

$$U = \left[\frac{1}{h_f} + \frac{1}{\frac{\lambda_m}{\delta_m} + \frac{JH_v}{T_{fm} - T_{pm}}} + \frac{1}{h_p} \right]^{-1} \quad (4)$$

U , δ , and λ_m are the overall heat transfer coefficient, membrane thickness, and membrane thermal conductivity, respectively. A model differs based on how h_p and h_f are estimated from one of numerous Nu correlations (where $Nu = hD_h/\lambda$), which depend on the module geometry and flow conditions. The flow through the DCMD module used in this work was

modeled as laminar, undeveloped flow between two flat plates. This problem has been solved via numerical methods by Kays et al. [15] for a variety of surface heating conditions. Nu values were calculated along the module length in 1-mm increments and integrated to calculate an average Nu along the length of the module. The temperatures at either side of the membrane surface T_{fm} and T_{pm} determine the driving force for mass transfer, and because $q_f=q_m=q_p$, they can be expressed analytically in terms of membrane properties and bulk temperatures as

$$T_{pm} = \frac{\lambda_m / \delta_m (T_p + (h_f / h_p) T_f) + h_f T_f - J H_v}{\lambda_m / \delta_m + h_f (1 + \lambda_m / (h_p \delta_m))} \quad (5)$$

$$T_{fm} = \frac{\lambda_m / \delta_m (T_f + (h_p / h_f) T_p) + h_p T_p + J H_v}{\lambda_m / \delta_m + h_p (1 + \lambda_m / (h_f \delta_m))} \quad (6)$$

T_p , T_f , and the flow velocity are set operating parameters, whereas δ , λ_m , and H_v can be found in literature or estimated. h_p and h_f are estimated from the Nusselt number correlation described earlier.

As with heat transfer, mass transfer occurs in three steps: through the feed-side boundary layer, through the membrane, and through the permeate boundary layer. The ΔP_{vap} is a function of the composition and water temperatures on the membrane surface (T_{fm} and T_{pm}) and is determined by using the Antoine equation, accounting for the activity of the water with solutes present. It is this value that is the driving force for mass transport across the membrane. The transport of gases through porous media has been studied extensively, and there are a number of theoretical models available. The mean free path of water vapor through the pore matrix is used as a guideline for determining the appropriate transport mechanism and is given by $l_i = k_B T / 2.5 p p s_i^2$. For water vapor at 30 °C under atmospheric pressure, the mean free path is ~0.12 mm. Comparing the mean free path to the pore diameter determines if Knudsen or molecular diffusion is the dominant transport mechanism (that is, if molecule-wall or molecule-molecule collisions are more important). If $l_i < d_p < 100l_i$, both mechanisms must be accounted for. With d_p ranging from 0.2~0.45 μm for the membranes used in this study, the membranes used in our system fall under the combined Knudsen molecular diffusion mechanisms. Phattaranawik et al. [16] give the combined Knudsen molecular vapor flux across a membrane as

$$J = \frac{(\epsilon / \chi) P_T D_{m, w}}{\delta_m R T_m} \times \ln \left(\frac{D_{Kn} (P_T - P^{vap}_p) + (\epsilon / \chi) P_T D_m}{D_{Kn} (P_T - P^{vap}_f) + (\epsilon / \chi) P_T D_m} \right) \quad (7)$$

where

$$D_{Kn} = \frac{4}{3} \frac{\epsilon d_p}{\chi} \sqrt{\frac{R T_m}{2 \pi M_w}} \quad (8)$$

and

$$P_T D_m = 1.895 \times 10^{-5} T^{2.072} \quad (9)$$

Because J , T_{fm} , and T_{pm} , are coupled, an iterative approach is taken to find a solution by using the solver function in Excel; results from this approach are presented in Chapter 2.

1.4 Temperature Polarization

In membrane distillation, heat may be transported across a membrane either in the form of latent or convective heat [9]. Latent heat transfer results from the evaporation of liquid across the membrane and cannot be eliminated, as it is the basis for the operation of the process [5, 7, 17]. However, because conductive heat is transferred through the membrane material and the pore gases, it may be reduced through changes in membrane structure such as porosity and thickness. Heat losses of any kind reduce process efficiency through the formation of thermal boundary layers at the membrane interfaces with the feed and permeate solutions and also result in the loss of the process driving force (namely, a decrease in feed temperature along the length of the membrane). Thermal boundary layers reduce the temperature gradient between the feed and condensing solutions, and ultimately reduce system performance [5, 8, 18]. The significance of the thermal boundary layer is quantified in terms of the temperature polarization coefficient, TPC, which is the ratio of useful energy for mass transfer to the total energy invested in the process and is written as Equation 8:

$$TPC = \frac{T_{fm} - T_{pm}}{T_f - T_p} \quad (10)$$

Because permeate flux is primarily a function of the temperatures at the membrane surfaces and not of the bulk temperatures, it is desirable to have the difference between T_{pm} and T_{fm} be as high as possible, and $T_f - T_p$ is the upper bound on this difference. In other words, the TPC should be as close to unity as possible. However, in most cases the TPC is lower than unity and varies between 0.2 and 0.9 [5]. Temperature polarization may, however, be minimized by reducing the conductive heat loss through the membrane, which reduces T_{pm} while maintaining a high T_{fm} .

1.5 Membrane Distillation/Reverse Osmosis Energy Comparison

The feasibility of a new technology will ultimately depend on whether it provides significant advantages over established technologies. An ideal candidate utility would be one that already has methane gas production capability, through anaerobic digestion as either the primary treatment of wastewater or as for solid digestion of waste sludge in an aerated WWTP. The methane generated could be burned to provide the driving force necessary for mass transport in an MD system. The utilization of such waste heat to drive an MD process, rather than the comparatively large amounts of electricity (available at a higher cost than the waste heat) necessary to generate high pressures in an RO plant, makes MD a competitive alternative to established desalination technologies such as RO. The two dominant technologies used in desalination are RO and multistage flash distillation (MSF), which account for approximately 54 and 30% of the market share for desalination worldwide [19]. Of the two processes, MSF is much more energy intensive, consuming 26.4 kWh per m³ of water produced, whereas RO consumes 5–7 kWh per m³ of water produced, when the feed is seawater (20, 21). Membrane processes and RO in particular are predicted to continue to gain market share; therefore, any new technology will have to compete with RO. The average cost to desalinate seawater using RO is \$0.47/m³ [19]. If one assumes an electricity cost of \$0.05/kWh, this means that nearly half of the cost to produce water stems from the energy requirements. Although MD is not as mature a technology as RO, it is predicted to be competitive from an energy standpoint. One pilot study shows that the energy requirements

for MD are between 22 and 67 kWh/m³ [20]. Table 1.2 shows a comparison between RO- and MD-based energy magnitudes and types.

Table 1.1. Desalination Technology Energy Comparison^a

Energy Source	Reverse Osmosis, kWh/m ³	Membrane Distillation (High), kWh/m ³	Membrane Distillation (Low), kWh/m ³
Electrical	4.5	0.75	0.75
Heat	0	22	67

^aBoth high and low estimates are included for membrane distillation [20].

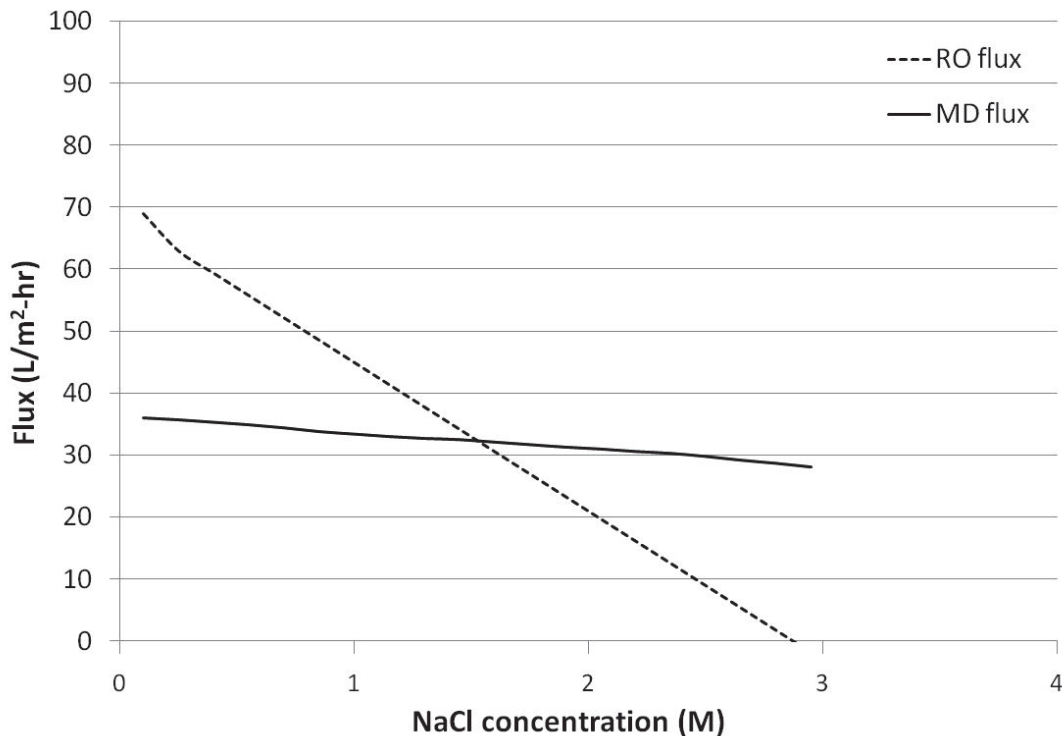


Figure 1.3. Flux as a function of ionic strength for hypothetical RO and MD modules.

At first glance, a comparison of RO and MD absolute energies seems to strongly favor RO. However, the effect of increased osmotic pressure as well as the cost of each energy source must be considered. Figure 1.3 illustrates the effect of increased osmotic pressure on two theoretical membrane modules.

The graph shows that, for a given energy input, increasing the feed ionic strength has a much greater impact on the flux of the RO module. The phase change from liquid to vapor means that osmotic back pressure is not a factor in membrane distillation. In real-world systems, RO operation compensates for high-concentration feed waters by increasing the hydraulic

pressure to maintain a constant flux, which constitutes the bulk of the electrical energy requirement. This pressure increase would not be required for MD operation.

A second and equally important consideration is the cost of the energy for each technology. While all of the energy for separation in an RO system is derived from high-cost electricity, the bulk of the energy needed in an MD system is thermal; so the cost comparison favors MD if cheaper sources of heat can be used to drive separation. Figure 1.4 provides estimates for each technology, giving two scenarios for the MD energy source.

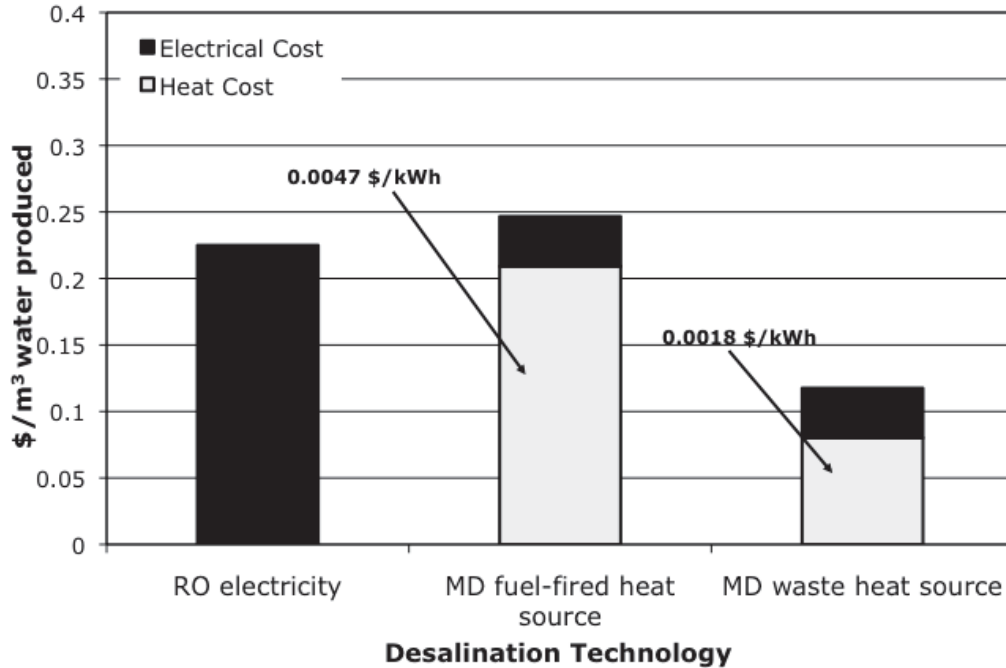


Figure 1.4. Cost comparison between RO and MD technologies assuming energy consumption at midpoint of 44.5 kWh/m³ and two different heat sources.

Figures 1.3 and 1.4 illustrate that MD technology has the potential to save money in circumstances where the treatment of high-concentration water is necessary and/or a cheap source of thermal energy is readily available. These conditions often exist in applications where water reuse is required, such as concentration treatment/disposal, tertiary wastewater treatment, industrial settings, and so on.

Chapter 2

Ceramic Membrane Surface Modification

2.1 Membrane Materials for Membrane Distillation

To date, polymeric membranes have most widely been studied for use in MD applications, with polyvinylidene difluoride (PVDF) and PTFE being the most commonly studied materials [11, 14, 21, 22]. The performance of different polymeric membranes in various MD configurations is summarized in Table 2.1.

Table 2.1. Summary of Water Fluxes Measured by Previous Researchers Investigating Direct Contact Membrane Distillation and Vacuum-Enhanced Membrane Distillation

Reference	Application	Membrane Material	Feed Specifics	Water	Avg Water Flux (L/m ² h)
14	DCMD	PP	$\Delta T = 60\text{ }^{\circ}\text{C}$, 7.6 mg/L TDS		29.17
24	DCMD	PP	$\Delta T = 70\text{ }^{\circ}\text{C}$, 10% NaCl		50
25	Vacuum-enhanced DCMD	PTFE	$\Delta T = 20\text{ }^{\circ}\text{C}$, 600 mg/L NaCl		35
26	VMD	PTFE	$\Delta T = 25\text{ }^{\circ}\text{C}$, Seawater		5.40
27	DCMD	PTFE	$\Delta T = 30\text{ }^{\circ}\text{C}$, DDW ^a		14.40
28	DCMD	PVDF	$\Delta T = 40\text{ }^{\circ}\text{C}$, 20 mM humic acid		36.27
29	DCMD	PVDF	$\Delta T = 5\text{ }^{\circ}\text{C}$, Distilled water		5.76

^aDDW, doubly deionized water; VMD, vacuum-enhanced membrane distillation. Reported values were obtained for different experimental flow rates, module geometries, and membrane characteristics.

The range of water fluxes reported (5.4–50 L/m²-h) by each group in Table 2.1 is attributed to differences in operating conditions (temperature and feed water chemistry), module design (each with an associated performance efficiency), and membrane properties. Unfortunately, it is difficult to control the pore structure, geometry, and size distribution during the fabrication

of polymeric membranes, which results in most polymeric membranes being characterized by tortuous and irregularly shaped pores. Furthermore, polymeric membranes exhibit a number of deficiencies when compared to ceramic ones with regard to performance in harsh environments [23], such as those characteristic of potential feed waters for MD. Such deficiencies include the sensitivity of polymeric materials to extreme temperatures and pHs and to oxidants like chlorine. The sensitivity of polymeric materials to aggressive or oxidizing agents also limits the types of chemicals that may be applied to rigorously clean fouled membranes or to prevent scaling or biological growth, which are concerns in nearly all desalination processes. Using ceramic membranes in place of polymeric ones in MD applications is therefore an interesting proposition. Ceramic membranes offer numerous advantages that make them an attractive option for use in MD applications, such as a high mechanical strength, high chemical and oxidant tolerance, and thermal resistance. These properties collectively allow ceramic membranes to be used under harsher conditions than those for polymeric membranes, thereby expanding MD applications.

2.2 Ceramic Surface Modification

Metal oxides of alumina, zirconia, silica, iron, and titania are commonly used for the fabrication of ceramic membranes [24-26]. Ceramic membranes tend to be hydrophilic because of the hydroxyl groups that characterize metal oxide surfaces; consequently, water is readily absorbed into the ceramic pore matrix [27]. This characteristic has traditionally made ceramic membranes unsuitable for separation processes such as MD and pervaporation, where it is critical that a vapor-liquid boundary be maintained at the pore interface. A number of methods have been used to modify ceramic materials so as to make them hydrophobic [26-33]. The same hydroxyl groups that make them initially hydrophilic also allow them to be readily modified via substitution with hydrophobic moieties. Three different hydrophobic polymers for modifying the surface chemistry of the ceramic membranes were investigated: $^1\text{H}, ^1\text{H}, ^2\text{H}, ^2\text{H}$ -perfluorodecyltriethoxysilane (PFS), trichloromethylsilane (TCS), and trimethylchlorosilane (TMS). Commercially available alumina anodisc membranes were used to evaluate the effectiveness of the different surface modification techniques on ceramic membranes.

2.3 Hydrophobic Solution Grafting

The PFS grafting solution was prepared by dissolving the chemical in chloroform so as to make a 10 mM solution according to the method outlined by Krajewski et al. [28]. The TCS and TMS grafting solutions were prepared by dissolving the respective polymers in analytical-grade toluene to produce a 2.5% (w/w) solution. The success of the grafting procedure was assessed via contact angle measurements and Fourier transform infrared (FTIR) spectroscopy; atomic force microscopy (AFM) and scanning electron microscopy (SEM) imaging were used to determine pore structure impacts. Figure 2.1 shows the contact angle of a 5- μL water droplet before and after grafting. Figure 2.2 shows FTIR spectroscopy results from PFS- and TCS-coated anodisc membranes. Figure 2.2a and b indicate the changes to surface chemistry of the alumina membranes. Membranes grafted with TMS showed no changes in FTIR spectra and thus are not shown. These results verify contact angle measurements of doubly deionized water (DDW) on the modified membrane surfaces: 141°, 134°, and 30°, for PFS, TCS, and PFS, respectively. The TMS-coated membranes failed to reach sufficient hydrophobicity levels (>90° contact angle) and were not analyzed further. The treated membranes were also characterized via SEM imaging, as presented in Figure 2.1a and b. Figure 2.3 shows SEM images of an unmodified anodisc membrane as well as those

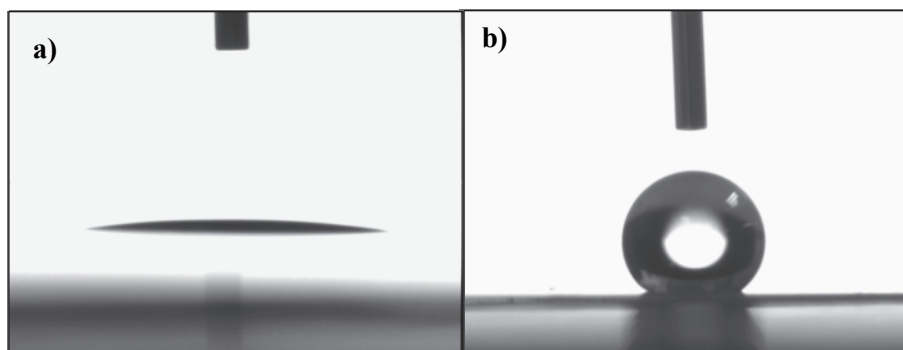


Figure 2.1. Contact angle measurement of anodisc (a) before and (b) after PFS grafting.

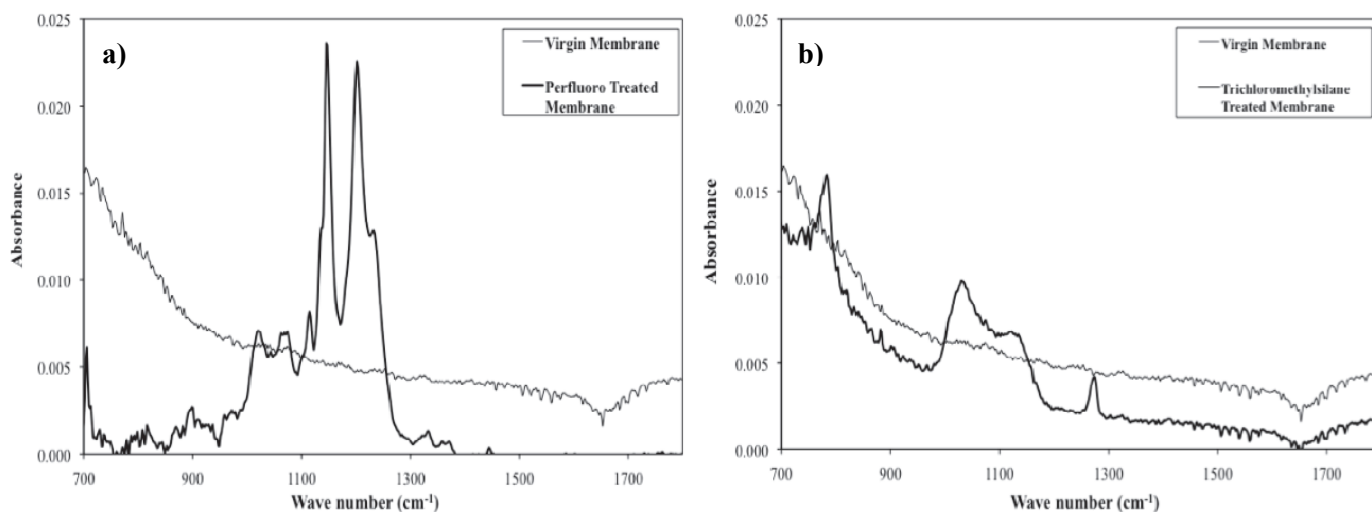


Figure 2.2. FTIR absorbance spectra of 200-nm alumina anodisc membranes with surface treatments of (a) PFS and (b) TCS. The FTIR spectra for an unmodified anodisc membrane are included in each figure for comparison.

grafted with TCS and PFS. Pore blockage using TCS is clearly evident in the images when compared with the untreated membrane, whereas the PFS grafting method appears to have left the original structure intact. Membranes were further characterized by stirred cell tests to measure permeability as well as liquid entry pressure, which is an important indicator of the operating limits of the membrane. Membrane coupons were prepared for stirred cell tests by securing the membrane samples in a plastic support with silicone glue. This arrangement provided structural support to the membranes and allowed a watertight seal to be formed in the test cell. The membrane/support assembly had an active membrane area of 531 mm².

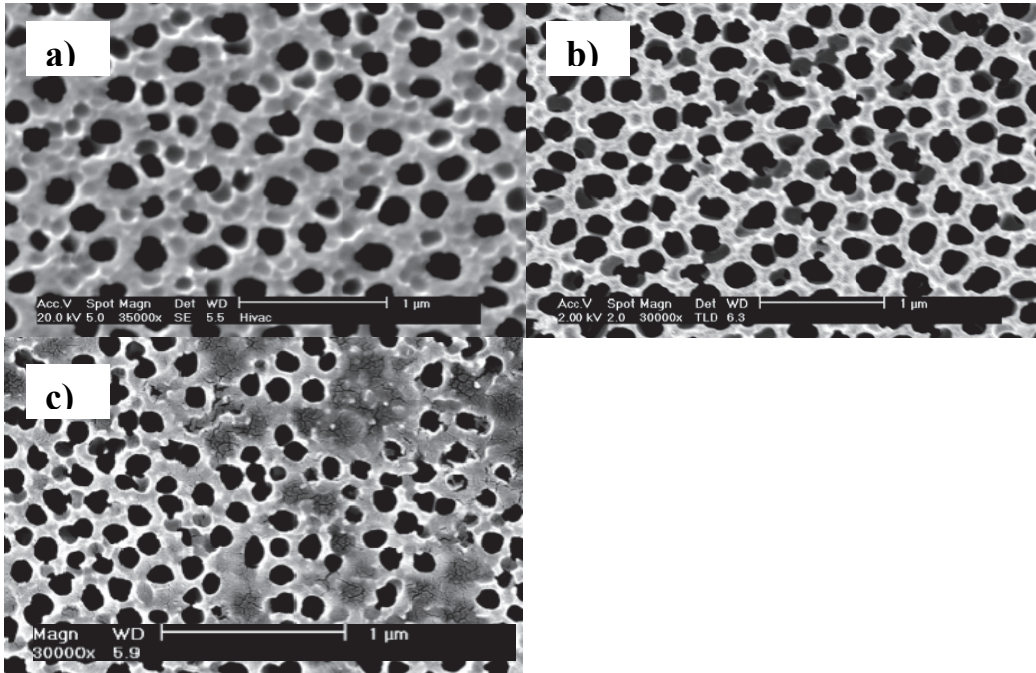


Figure 2.3. Representative SEM images of (a) an unmodified anodisc membrane and after coating with (b) PFS and (c) TCS grafting solutions.

2.4 Membrane Characterization

A thorough characterization of the physical and chemical membrane properties is necessary to compare their performance. This task was accomplished by subjecting the PTFE, PFS, and TCS membranes to a variety of quantitative measurements.

2.5 LEP Measurements

The liquid entry pressure (LEP) is a critical membrane characteristic for MD as it represents the pressure at which liquid water will flood the membrane pores. Once the pores are flooded, solutes may pass from the feed directly to the product stream. It is therefore critical to MD that the operating pressure, which is a function of temperature, ionic strength, fluid flow rate, and module geometry, be lower than the LEP of the membrane. The relationship between the LEP and relevant system characteristics is shown in the Laplace (Cantor) equation [11, 34]

$$P_{liquid} - P_{vapor} = \Delta P = \frac{-2B\gamma_L \cos\theta}{r_{max}} < LEP \quad (11)$$

where B is a geometric factor for which a value of 1 indicates circular pores, γ_L is the liquid surface tension, θ is the liquid–solid contact angle, and r_{max} is the largest pore radius. In MD processes, operating at high Reynolds numbers allows for increased mixing and improved

mass transfer [35] but can also lead to operating pressures that exceed the LEP. In addition, both the process conditions and the feed water composition will affect γ_L [36]. Salt content will increase γ_L ; conversely, γ_L decreases with increasing temperature and with the presence of surfactants in solution. In Equation 11, B and r_{max} are determined by membrane structure and indicate areas where engineering design can improve membrane performance in an MD process. The LEP is measured by slowly increasing the air pressure to a column of water on one side of the membrane until the first drop of water emerging from the membrane is observed; the pressure at which this occurs is recorded as the LEP. This is schematically represented in Figure 2.4.

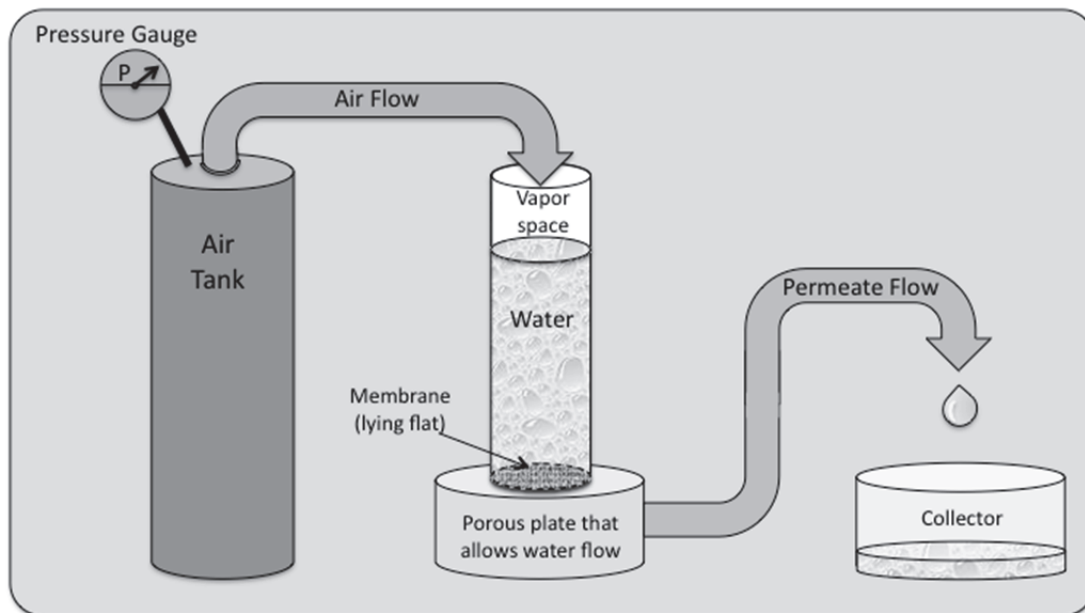


Figure 2.4. Schematic of LEP measurement for a disc membrane. The LEP is the pressure indicated on the gauge when the first drop of water permeates through the membrane.

LEP measurements taken while using DDW at 20 °C resulted in LEPs of 561 kPa (± 41), 545 kPa (± 88), and 246 kPa (± 21) for the PFS, TCS, and 200-nm Pall PTFE TF-200 membranes, respectively. Earlier work has shown that hydrophobic membranes with pore sizes of 0.2 μm had entry pressures between 200 and 400 kPa [35, 37]. The TF-200 membranes fall within this range, whereas the treated ceramics have a significantly higher pressure threshold for wetting. The greater LEP indicates that the ceramics will have greater flexibility for different operating conditions by allowing higher flow rates for increased mass transfer efficiency. Alternatively, the ceramic membranes may be better suited for treating feed waters, which would otherwise result in pore flooding as a result of the reduced surface tension of water at elevated temperatures or with a high surfactant concentration. Still another benefit of having a higher LEP would be that the membranes could be subjected to improved cleaning methods by increasing allowable pressures during water scouring of fouled membranes, thereby increasing the amount of foulant removed during each cleaning cycle.

2.6 TCS vs. PFS Membrane Surface Coatings

A number of other analyses were performed on the modified anodisc membranes in addition to the SEM imaging and FTIR spectroscopy. Surface area was determined with Brunauer-

Emmett-Teller (BET) adsorption isotherms measured via nitrogen adsorption by using a SA 3100 surface area analyzer (Beckman-Coulter, Fullerton, CA). A Digital Instruments Dimension 3100 AFM was used for roughness measurements (Veeco, Plainview, NY). Membrane permeability was also assessed by using a stirred cell (Sterlitech Corp., Kent, WA). Liquid water flux was measured for 1 h at five different pressures. Water flux was plotted as a function of pressure, and permeability was calculated by regression analysis. Table 2.2 summarizes results from the various characterization analyses.

Table 2.2. Measured and Calculated Values of the TF-200 and Anodisc Membranes Modified using PFS and TCS

Membrane	LEP, kPa	Water Permeability, L/m ² -h-bar	r_{max} , nm	Pore Geometry Factor, (B) ^a	BET surface area, m ² /g	AFM R_{RMS} , nm
TF-200	246 ± 21	1.77	450	0.55 ± 0.05	NA	NA
PFS 200-nm anodisc	561 ± 41	0.96	290	0.97 ± 0.08	3.90	30.8
TCS 200-nm anodisc	545 ± 88	1.46	NA	NA	3.67	21.7

^aCalculated from the Laplace (Cantor) equation: $\Delta P = -2B \cos \theta / r_{max} < LEP$.

The BET surface area and AFM root mean square roughness (R_{RMS}) measured for the modified anodisc membranes both show that TCS has a significantly greater impact on these parameters than the unmodified values of 4.12 m²/g and 32 nm, respectively. These results verify the SEM images presented in Figure 2.3, which showed significant pore blockage for the TCS-coated membranes. A comparison of the membrane water permeability measured in a stirred cell shows that both modified ceramics give values similar to the polymeric TF-200 membrane. The LEP values, measured contact angles, and estimated pore sizes for the membranes were used as input into the Laplace (Cantor) equation to calculate the pore geometry factor B . The TCS membrane was deemed unsuitable for further evaluation because of the pore blockage noted earlier. The B value for the anodisc membrane of 0.97 ± 0.08 is much closer to unity than is the value of 0.55 ± 0.05 for the TF-200 membrane. A B value of 1 indicates perfect circular pore openings, and this result is verified by the Figure 2.5 SEM images of an anodisc and TF-200 membrane. From the figure, it is clear that the anodisc is characterized by a circular pore structure, whereas the TF-200 membrane pore geometry is much more irregular. The irregular shape of the TF-200 membrane pores, coupled with the likely larger r_{max} for this membrane, results in the LEP being lower than that measured for the anodisc membrane.

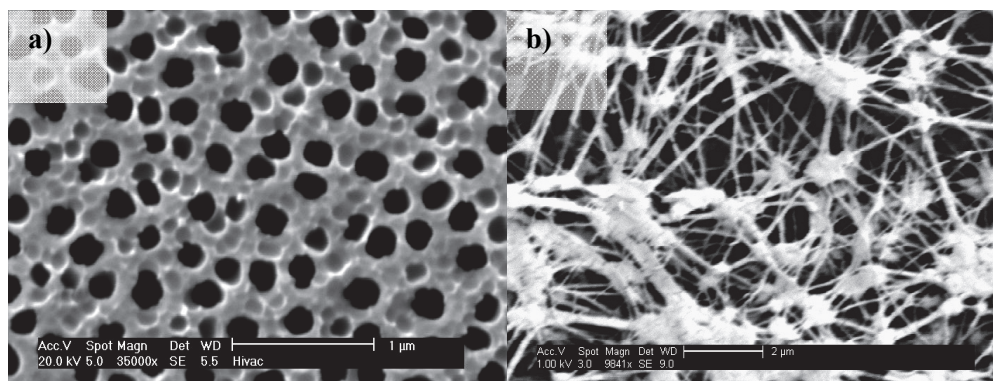


Figure 2.5. Representative SEM images of (a) an unmodified anodisc and (b) a TF-200 membrane surface. Both membranes have a reported mean pore diameter of 200 nm.

2.7 Membrane Durability

Important aspects of membrane performance include resistance to physical and chemical stresses, which will impact the effectiveness and useful life of a membrane module. Ceramic membranes are noted for their mechanical robustness, resistance to deformation at high temperatures, and inert chemical nature but can be brittle and prone to cracking. Experiments were performed to investigate both the chemical and mechanic properties of the membranes.

2.8 Ceramic Membrane Tensile Strength

Unmodified and PFS-treated anodisc membranes were subject to stress–strain measurements using a RSA III Micro-Strain Analyzer (TA Instruments, New Castle, DE). Tests were done by cutting rectangular pieces of anodisc membranes and taking their measurements in the x , y , and z directions. The samples were placed in the instrument, and an incremental tension force was applied until sample breakage. The ratio of the stress and strain in the initial linear portion of the curves can be used to calculate the Young’s modulus for both membrane samples. The Young’s modulus is defined as follows:

$$E = \frac{\sigma}{\varepsilon} \quad (12)$$

where E , σ , and ε represent the Young’s modulus, tensile stress, and tensile strain, respectively. The Young’s modulus for the unmodified and PFS-coated anodisc membranes is calculated to be 6.0 and 1.9 MPa, respectively. This 68% decrease suggests that the modification has a significant impact on the membrane physical properties. This loss of membrane strength after modification is a concern and may impact operation. To address this issue, a review of the surface coating procedure was undertaken. Laboratory observations of membranes that had been soaked in grafting solutions but not heated did not appear to show increased brittleness, suggesting that the heat treatment, rather than the surface coating, was responsible for the increased brittleness. Under this assumption, the coating procedure was varied and the membrane strength measured. The original coating procedure requires four successive grafting periods of increasing exposure to the PFS solution, each followed by a 12-h drying interval at 100 °C. The drying time was adjusted for this investigation by reducing it to 6, 3, and 1 h. The RSA III Micro-Strain Analyzer (TA Instruments) was again used on membrane coupons. Tests were done by cutting rectangular pieces of anodisc membranes and taking their measurements in the x , y , and z directions. The samples were

placed in the instrument, and an incremental tension force was applied until sample breakage. The results of these tests are shown in Figure 2.6 in addition to the initial values.

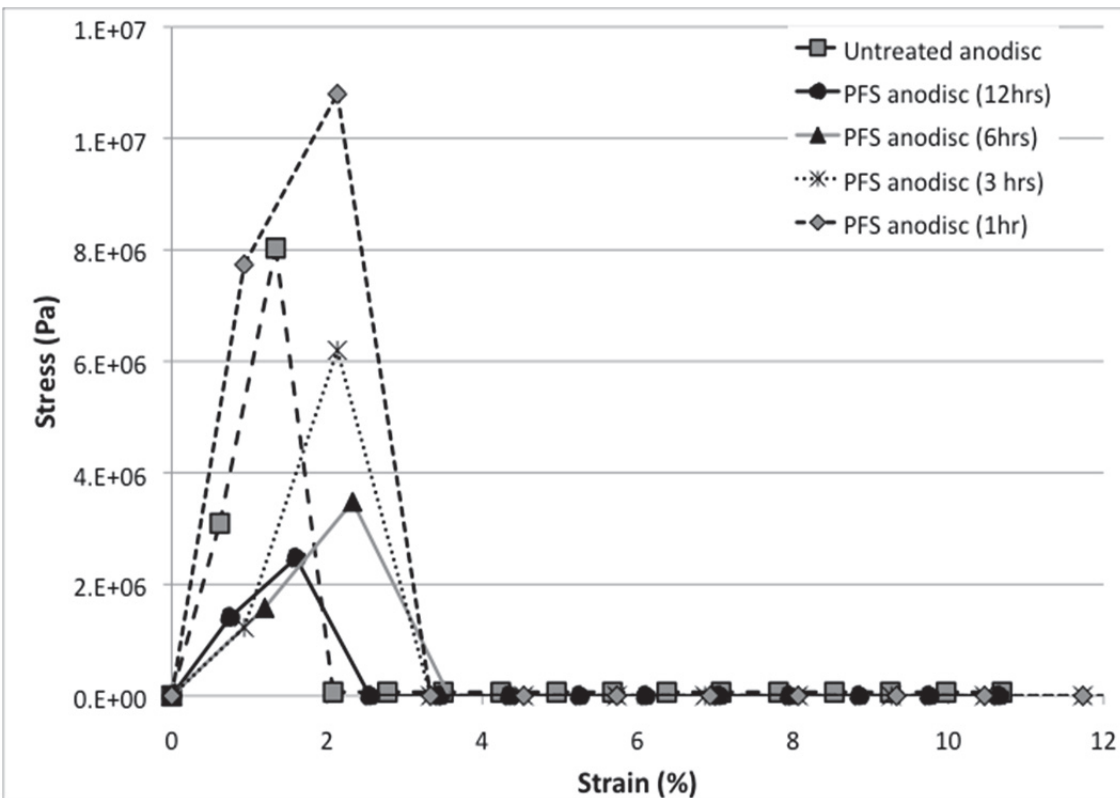


Figure 2.6. Stress–strain curves for unmodified and PFS-treated anodisc membranes exposed to different drying times.

The curves clearly show that loss of membrane strength is closely correlated to the drying time and confirms our initial hypothesis. A calculation of the Young’s modulus ($E = \sigma/\epsilon$) for each curve allows each to be directly compared. The values of the Young’s modulus are 1.9, 1.5, 2.9, and 5.1 MPa for anodisc membranes subject to 12-, 6-, 3-, and 1-h drying times, respectively. The Young’s modulus for untreated anodisc membranes is 6.0, which means that reducing the drying time to 1-h intervals results in only a 15% reduction in membrane strength. In addition, no loss of hydrophobicity was observed.

The stronger membranes exhibited a dramatically reduced breakage rate. Although the improved strength is a promising development, it does not fully address the membrane strength issue as it relates to the hydrodynamic cleaning treatments. However, we believe this issue is isolated to bench scale, as commercial α or β alumina oxides are stable above 1000°C.

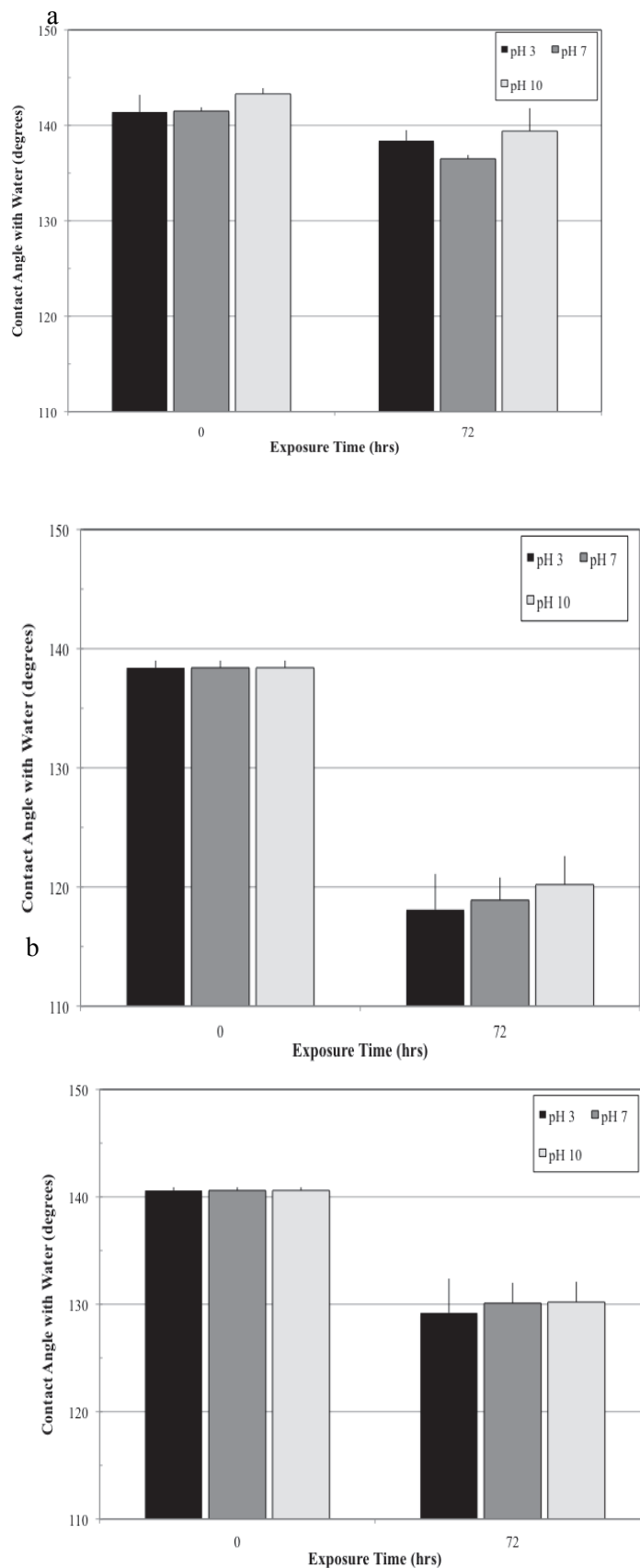


Figure 2.7. Angle of contact with water as a function of exposure time to a 2.82 mM free chlorine solution at three different pHs for (a) a PFS-treated anodisc membrane, (b) a TCS-treated anodisc membrane, and (c) a TF-200 membrane ($T=20\text{ }^{\circ}\text{C}$, $n=3$). Note that $t=0$ indicates the initial contact angle measurement prior to exposure to the chlorine solution.

2.9 Membrane Resistance to Chlorine

The chlorine tolerance of the TF-200 and modified anodisc membranes was assessed by using solutions of sodium hypochlorite (NaOCl). The NaOCl solution was made with a concentration of 2.82 mM (100 ppm) as free chlorine. The solution pH was adjusted to either pH 3, 7, or 10 by adding appropriate amounts of hydrochloric acid (HCl) or sodium hydroxide (NaOH). The membranes were submerged in the chlorine solution and kept in the dark. The solution was changed every 24 h so that a constant chlorine concentration was maintained. Periodically, the membranes were removed, rinsed with DDW, and allowed to dry. On drying, the membrane angle of contact with water was measured. The membranes were then placed back in the chlorine solution. The test was ended after 72 h of exposure. Changes in the membrane's angle of contact with water as a function of exposure time were used as an indicator for oxidation of the functional groups on the membrane surface. Additionally, SEM imaging analysis of the membrane surfaces before and after exposure to the chlorine solution was used to identify if any physical damage to membrane structure had resulted from exposure to the chlorine solution.

The angles of contact with water before and after exposure to the chlorine solution (2.82 mM free chlorine) and at pHs of 3, 7, and 10 are shown in Figure 2.7. A loss of hydrophobicity (namely, a decrease in contact angle) was assumed to be indicative of degradation of the surface groups. Contact angle has not to our knowledge been correlated to oxidation. However, membrane characteristics key to the DCMD process are contact angle and membrane structure—any changes to these two properties resulting from exposure to a chlorine solution are of interest. In this case, if the surface groups were becoming oxidized, then a gradual hydrophilization (namely, decreasing angle of contact with water) of the membrane surface should be evident, either through removal of the surface groups and subsequent exposure of the ceramic surface or through oxidation and transformation of the groups themselves. We note here that 110° was selected as a pseudo “zero” value for the y axis in Figure 2.7 because it is the approximate contact angle at which we calculate pore flooding of the TF-200 to occur during MD operation at 20 psi, which is a typical line pressure at which we expect a real-world MD system to operate.

The data from these tests show that the PFS-treated membranes have the highest resistance to chlorine degradation, with only a $3.9 \pm 1.5^\circ$ decrease in contact angle following 72 h of exposure, followed by the TF-200 membranes ($10.7 \pm 0.5^\circ$ decrease) and lastly the TCS-treated membranes ($19.3 \pm 1.1^\circ$ decrease). In all cases, the membranes retained sufficient hydrophobicity for continued MD operation and the contact angle decreased by no more than 3° after the 1st h of exposure, indicating that little degradation occurred after this initial period. Typical chlorine doses used to prevent biofouling are 0.0282 mM for continuous exposure and 1.41 mM for shock treatment [38]. These results indicate that all three membranes would be capable of tolerating longer exposure times at more effective concentrations than would typically be used to control biofouling.

2.10 Membrane Performance Comparison

We used two methods of comparing membrane performance.

2.11 Membrane Distillation Module

Evaluating the performance of the anodisc and PTFE membranes during MD operation in a bench-scale unit was accomplished by using a bench-scale module. The test unit consists of the following: water chiller and heater, peristaltic pumps, flowmeters, in-line thermocouplers, pH and conductivity probes, a mass balance, stir-plates, and a flat-sheet test cell. The test cell has a plate-and-frame configuration, which allows for either cocurrent or countercurrent flows of the condensing and feed streams on opposite sides of the membrane. Ion rejection is measured by using conductivity probes. A schematic of the test unit is given in Figure 2.8.

2.12 Model Validation and Ceramic/Polymeric Performance Comparison

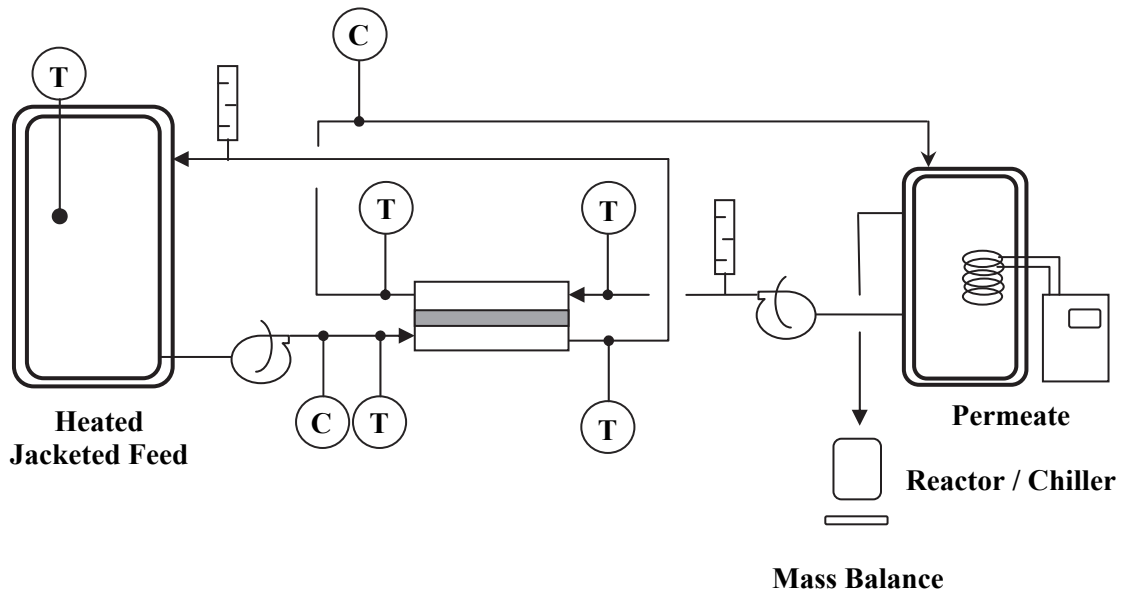


Figure 2.8. Schematic showing the DCMD bench-scale test unit used in this investigation (C=conductivity probe, T=temperature probe). Water flux through the membrane is quantified by measuring the overflow from the permeate reactor by using a mass balance.

Equations 1–9 were solved iteratively by using the Excel solver function for given input flow and temperature conditions to model the heat and mass transport of the DCMD module. The results in Figure 2.9a and b show the model performance along with corresponding observations of DCMD experimental results for both the TF-200 and PFS membranes tested.

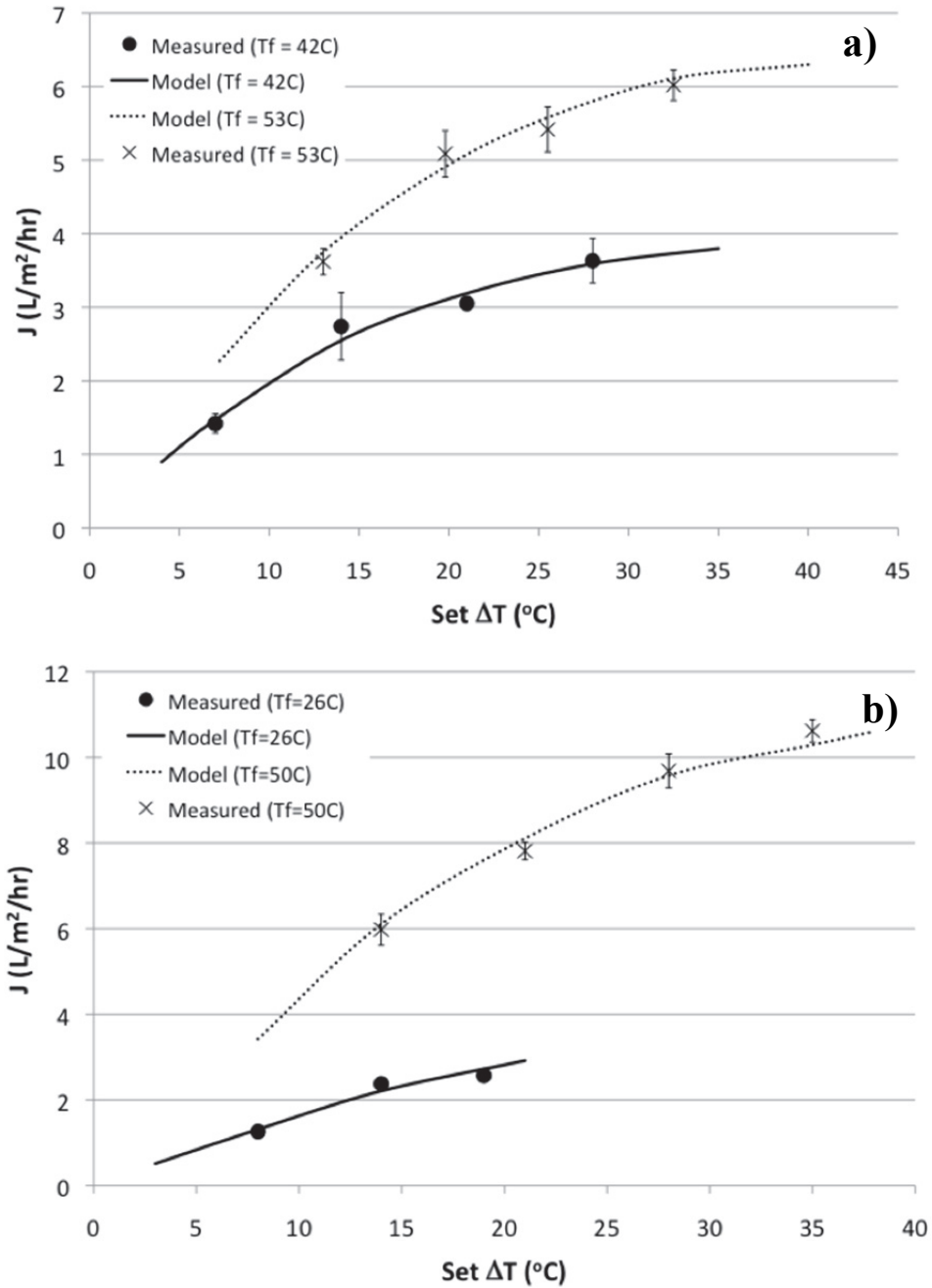


Figure 2.9. Water flux across (a) PFS anodisc and (b) TF-200 membranes during DCMD of DI water as a function of feed/permeate temperature difference. Data points are grouped by feed temperature.

Each data point is the average of between four and six flux readings at the specified operational conditions, and the error bars indicate measurement variation. The model fits the experimental data quite well for both types of membranes at different feed temperatures and ΔT values, with R^2 values of 0.99 calculated for both membranes. There are a number of other interesting observations to be made from Figure 2.9. The feed temperature had a much greater influence on the magnitude of the flux relative than did the temperature difference across the membrane, which has been noted elsewhere [16, 39] and is due to the exponential increase in vapor pressure with temperature.

The TF-200 membrane flux performance was superior to the PFS anodisc membrane's. The model can be used to compare flux performance at identical conditions (not shown) to demonstrate that flux values for the TF-200 membrane are ~45% above PFS 200-nm values. There are a number of differences between the anodisc and PTFE membranes, and the model parameters can be isolated and adjusted to explain the relative effects of each on membrane performance. Table 2.3 shows the relative effects of membrane porosity, thickness, and thermal conductivity on membrane flux and gives the theoretical flux of the PFS anodisc membranes when one substitutes the PTFE values. For example, the largest contributor to the lower flux of the PFS membrane is not the higher thermal conductivity ($\lambda_{\text{PFS200}} = 0.53 \text{ W/[m - K]}$) versus $\lambda_{\text{PTFE}} = 0.17 \text{ W/[m - K]}$) but rather the lower porosity of the PFS membrane ($\epsilon_{\text{PFS200}} = 0.4$ versus $\epsilon_{\text{PTFE}} = 0.65$).

Table 2.3. Theoretical Flux for PFS 200-nm Anodisc Membranes Calculated Incorporating Physical Characteristics from the TF-200 Membranes Used in This Study^a

Porosity, ϵ	Thickness, δ (μm)	Thermal Conductivity, λ ($\text{W/m}^2/\text{K}$)	Water Flux, J ($\text{L/m}^2/\text{h}$)
0.4	65	0.53	5.5
0.6*	65	0.53	9.9
0.4	65	0.17*	7.8
0.4	125*	0.53	3.9
0.4	65	0.53	7.0

^a*, value for TF-200 membrane. $J_{\text{PTFE}} = 10 \text{ L/m}^2/\text{h}$. All calculations made for $\Delta T = 30^\circ\text{C}$, $T_f = 50^\circ\text{C}$, and assuming an average membrane pore size of 200 nm.

Table 2.3 shows that the PTFE membrane possesses design characteristics that facilitate higher flux values. Of the physical parameters assessed, the only advantageous characteristic

of the PFS anodisc membrane is the thickness. The ability to assess and quantify the effects of different membrane parameters on performance can be valuable for membrane design. Future membrane design efforts should be directed toward areas that will produce the biggest payoff, allowing for the fabrication of a membrane possessing optimal physical characteristics. The ideal membrane will be thin and will have a high porosity and low thermal conductivity.

In summary, the results presented in this chapter highlight the difficulties associated with directly comparing membrane performances. Although ceramic membranes possess characteristics that would allow for harsher operating conditions, they also provide a lower flux than the TF-200 membranes. There will clearly be a tradeoff when selecting a membrane, as the higher flux values of the TF-200 will translate into a smaller module and therefore lower capital cost but also the possibility of operational costs higher than those of the PFS membranes. Further performance and economic studies are necessary to evaluate under what conditions these tradeoffs converge.

Chapter 3

Organic Matter Fouling in Membrane Distillation

3.1 Fouling in Membrane Distillation

Fouling is a ubiquitous problem in membrane processes. Pore blockage and cake layer formation on the membrane surface are phenomena that have been extensively studied for pressure-driven applications such as MF, NF, and UF [40-43]. Fouling is dependent on hydrodynamic conditions like shear rate, transmembrane pressure (TMP), and particle size, as well as on the solution chemistry, which includes feed concentration, pH, and ionic strength. There have been relatively few studies on fouling in MD processes to date. Culling the literature from 1980 to 2011 for the *Journal of Membrane Science* and *Desalination*, which are the primary journals for MD research, reveals that only about 5% of published literature on MD addresses the issue of fouling. This is so even though it is one of the key operational difficulties that will determine the feasibility of using this technology to treat a given feed water. This lack of rigorous investigation of fouling phenomena in MD represents an opportunity to make significant contributions to the knowledge in this technology.

The general lack of data on fouling in MD means that its impact on operation is not yet clearly understood [34]. Khayet et al. measured the flux of two kinds of membranes in a DCMD system treating humic acid feed solutions and found that fouling was higher at acidic pH values but was a minor issue overall when compared with pressure-driven processes [44]. They also determined that membranes with smaller pores and greater hydrophobicity exhibited a greater flux decline. In a different study, they concluded that humic acid fouling was independent of ionic strength with either NaCl or CaCl₂ [45]. These results are in disagreement with a study by Srisurichan et al., who found that, although fouling was negligible in the presence of NaCl, flux declined rapidly as the concentration of CaCl₂ increased [46]. Gryta studied the fouling of a DCMD module during the treatment of bilge water and meat-processing wastewater [47]. He determined that the flux decline stemmed mainly from the increased heat resistance caused by the fouling layer. The fouling layers were also characterized by using SEM images and FTIR spectroscopy. Another study examined iron scaling of an MD unit and found that the high porosity of the fouled layer caused a negligible flux decline but that using concentrated HCl to clean the deposits caused membrane pore wetting and subsequent flux decline [48]. Gryta examined the formation of alkaline deposits on an MD membrane during the filtration of tap water [49]. The deposits in this case caused a rapid flux decline, and SEM analysis showed that feed flow rate influenced deposit morphology such that larger and more compact crystals were noted at lower flow rates. A recent study showed that commercial antiscalants could be successfully applied to inhibit precipitative fouling [50]. Gryta et al. used MD to filter animal process wastewater and showed by energy dispersive x-ray spectroscopy and FTIR spectroscopy that the foulant layer was comprised primarily of protein and NaCl [51]. In summary, the available data on fouling MD are decidedly mixed, with some reports concluding that fouling is negligible, severe, or somewhere in between. It is clear, however, that a multitude of factors play a role in fouling, from membrane characteristics to solution chemistry.

3.2 Synthetic Foulants

The wide variety of organic foulants necessitates that a comprehensive investigation of membrane-fouling performance assess how different organic contaminants interact with the membrane. This will be accomplished by performing DCMD experiments using synthetic solutions of four different foulants to assess membrane fouling. The foulants studied were selected to provide a representative look at how various environmentally relevant constituents might affect filtration performance. Because this work ultimately examines the performance of DCMD filtering secondary treated wastewater, which contains a variety of organic particles and macromolecules, the foulants were selected to provide a method to estimate the fouling contribution of the different organic components.

3.3 Selection and Characterization of Model Foulants

The four foulants chosen are (a) humic acid, (b) sodium alginate, (c) bovine serum albumin (BSA) protein, and (d) carboxylate modified latex (CML) particles. Humic acid is the major component of natural organic matter (NOM) found in natural waters, comprising as much as 80% of the total organic matter [52]. In addition, humic acid has been shown to be a major contributor to flux decline in pressure-driven membrane systems [53, 54]. The majority of fouling studies concerning MD have measured humic acid as the primary foulant. Srisurichan et al. studied the effect of pH, divalent ion type, and ionic strength on humic acid fouling of an MD system [46]. Flux decline in the absence of ions was significant at pH = 3. At other pH values, flux decline was nearly negligible without the addition of ions, whereas the presence of NaCl caused only a slight flux decline and the addition of CaCl₂ resulted in a larger flux decline. The measured flux decline was significantly less than that observed for MF of the same waters. In two different studies, Khayet et al. measured the flux decline of PVDF and PTFE membranes in an MD system [45, 55]. They also found increased flux decline as the humic acid concentration increased, when CaCl₂ was present in the feed water, and when pH was lower; comparison showed that the flux decline was also less than that observed for a pressure-driven system.

Sodium alginate is a microbial polysaccharide often used as a model compound for extracellular polymeric substances (EPS), which are believed to contribute significantly to membrane fouling [56, 57]. Although the EPS found in waters are actually comprised of various polysaccharides, proteins, and nucleic acids, polysaccharides comprise a much larger fraction of alginate, making it a commonly used analogue for EPS. Alginate is formed by a 1-4-linked β -D-mannuronic acid, C-5 epimer, and α -L-guluronic acid [58]. Although there are numerous investigations of the behavior of alginate fouling in pressure-driven systems, its behavior in MD systems is unknown.

Proteins present in wastewater are yet another class of foulants of interest and will be modeled by BSA in the synthetic solutions to be tested. Ortiz de Zárate et al. filtered water at neutral pH with BSA concentrations ranging from 0.4 to 1% by using an MD process [59]. Two PTFE membranes having different pore sizes (200 and 400 nm) were tested. They found that, under the test conditions, fouling was nearly nonexistent, which they attributed to the low operational pressures (<0.1 atm). Conversely, the treatment of water containing protein in two other MD studies resulted in severe fouling, as evidenced by protein deposits on the membrane surfaces observed by SEM and FTIR measurements and by significant permeate flux decline [47, 51]. The proteins in the feed originated from meat-processing plants, so it is likely that complexity of the water resulted in constituents other than proteins contributing to the fouling, making it difficult to draw conclusions about the fouling potential of proteins.

The CML particles are synthesized via the copolymerization of carboxylate acids, are relatively hydrophilic, carry a negative charge, and are charge stabilized. Suspensions of these colloids are highly monodisperse and were selected to provide an easily characterized foulant to compare with the more-complex natural organic particles. In addition, this foulant provides information on the behavior of a purely colloidal foulant, because the prior three foulants are a mixture of particles and macromolecules.

3.4 Size and Zeta Potential Measurements

The size distribution and zeta potential of suspensions were measured by using a Malvern Zeta-Sizer (Worcestershire, England). Samples were prepared by first making a 50-mg/L solution. To facilitate aggregation, CaCl_2 was added to make a concentration of 0.01 M, and the pH was adjusted to 3, 7, or 10 by using HCl or NaOH. Before measurement, the solutions were filtered through a 1- μm -pore-size glass fiber filter to remove large colloids that would skew the measurement results. All measurements were done at 20 °C. A total of five measurements were taken for each set of pH conditions and are presented in Figure 3.1.

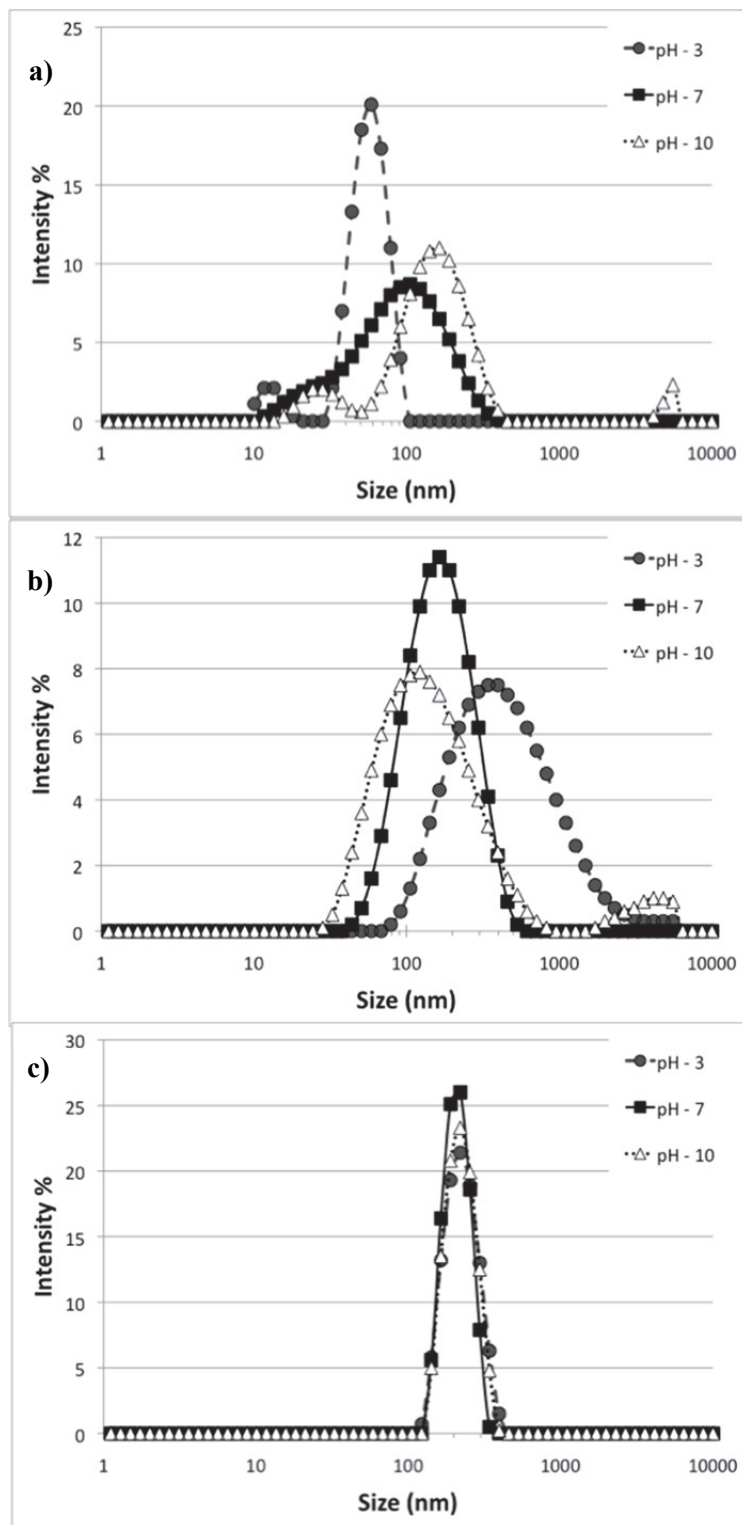


Figure 3.1. Representative intensity-weighted particle size distributions of (a) sodium alginate, (b) humic acid, and (c) CML colloids in 0.01 M CaCl₂ solutions at different pH values.

Figure 3.1 shows intensity-weighted particle size distributions of alginate, humic acid, and CML suspensions at different pH values. The mean alginate peak is smaller as the pH decreases but larger under basic conditions, whereas the converse holds for the humic acid suspension. This differing response of these suspensions to changing solution conditions illustrates the complexity associated with treating feed waters with different NOM components. In addition, to the shift in mean size, the shape of the intensity distribution changes under different pH conditions. At neutral conditions, the mean alginate peak is ~91 nm, with a slight bulge in the distribution in the 10- to 25-nm range. This region becomes more distinct at both pH extremes, with peaks at ~11 nm and ~24 nm for acidic and basic conditions, respectively. There is a third peak at less than pH = 10, at about 5500 nm, which suggests some rapid aggregation after filtration. For humic acid, there is not a secondary smaller peak at any pH, but there is a larger peak at 3500 nm at pH = 10. The CML particles are shown to be very stable particles, with similar intensity-weighted size distribution at all pH values. The manufacturer-listed size of the particles is 200 nm, and with peaks between 190 and 220 at different pH values, the particles clearly fall within this range. In addition, these suspensions show a much higher level of monodispersivity, as measured by the polydispersivity index (PDI), which was < 0.1 for nearly all measurements.

Although similar measurements were done for the BSA protein, the quality report for the measurements exhibited some irregularities, so the graph is not shown. Measurements taken at different concentrations did not yield better data. Table 3.1 summarizes the size/zeta potential measurements of the foulants. These data will be useful in describing differences between the membrane deposits. There are some general trends of importance here. All particles except for the CML beads show a general reduction in negativity of the zeta potential as the pH moves from acidic to basic conditions. CML is much more monodisperse at all pH values, which suggests that any changes in fouling observed can be attributed to changes in charge or other surface properties rather than to changes in size.

Table 3.1. Summary of Size and Zeta Potential Measurements for the NOM Suspensions To Be Used During Fouling Experiments^a

NOM Particle	Value for:		
	Z-avg size (nm)	PDI	Zeta Potential (mV)
Alginate	73 ± 9, 68 ± 1, 136 ± 22	0.32 ± 0.07, 0.33 ± 0.03, 0.34 ± 0.07	-17.6 ± 2.1, -11.2 ± 3.8, -5.1 ± 2.7
Humic acid	347 ± 22, 135 ± 0.0, 135 ± 37	0.33 ± 0.09, 0.25 ± 0.00, 0.36 ± 0.06	-18.1 ± 2.3, -10.4 ± 0.3, -10.8 ± 0.8
CML	223 ± 6, 209 ± 11, 212 ± 2	0.18 ± 0.03, 0.06 ± 0.06, 0.03 ± 0.03	-14.4 ± 0.9, -22.9 ± 1.5, -22.4 ± 0.9

^aAll measurements were performed in an electrolyte concentration of 0.01 M CaCl₂ and at T=20 °C and are displayed in order of ascending pH (3, 7, 10). The standard deviation is given for the average of 5 measurements.

3.5 Membrane Distillation Fouling Studies Using Model Foulants

The PFS anodisc membranes and PTFE membranes were tested in the MD module by using a temperature gradient of 35 °C and flow rate of ~140 mL/min for both the feed and condensing streams. Preliminary experiments agreed with results from the literature that indicate that NaCl as the solution electrolyte does not destabilize particles, as fouling was not observed when NaCl was used as the solution electrolyte. Therefore, a divalent cation, CaCl₂, was used throughout the experiments, which gives a closer approximation of the more-complex particle interactions that occur during the filtration of secondary wastewater. The concentration of CaCl₂ used during the tests was 0.01 M, which is within the range of ionic strengths found in wastewater [60]. MD filtration was evaluated at pHs of 3, 7, and 10 by adjustment of the feed water by using HCl or NaOH. The foulant concentrations were set to 50 mg/L to accelerate the fouling process during data collection. Each test was conducted for 24 h to ensure the collection of data that can accurately describe the initial evolution of fouling during MD operation. The foulants were added only after the flux had stabilized (approximately 30 min); this stable flux was used as the baseline for measuring flux decline over time and to reduce the effect of membrane variability. The feed solutions were prepared by first dispersing the foulant in the feed vessel. Once dispersed, the CaCl₂ was added, followed by pH adjustment.

3.6 Synthetic Fouling Studies

Figures 3.2 and 3.3 summarize the results from the synthetic organic foulant studies for both the PFS anodisc and TF-200 membranes, grouped by foulant type for each pH value measured. Each experiment was performed by using the DCMD module shown in Figure 2.8.

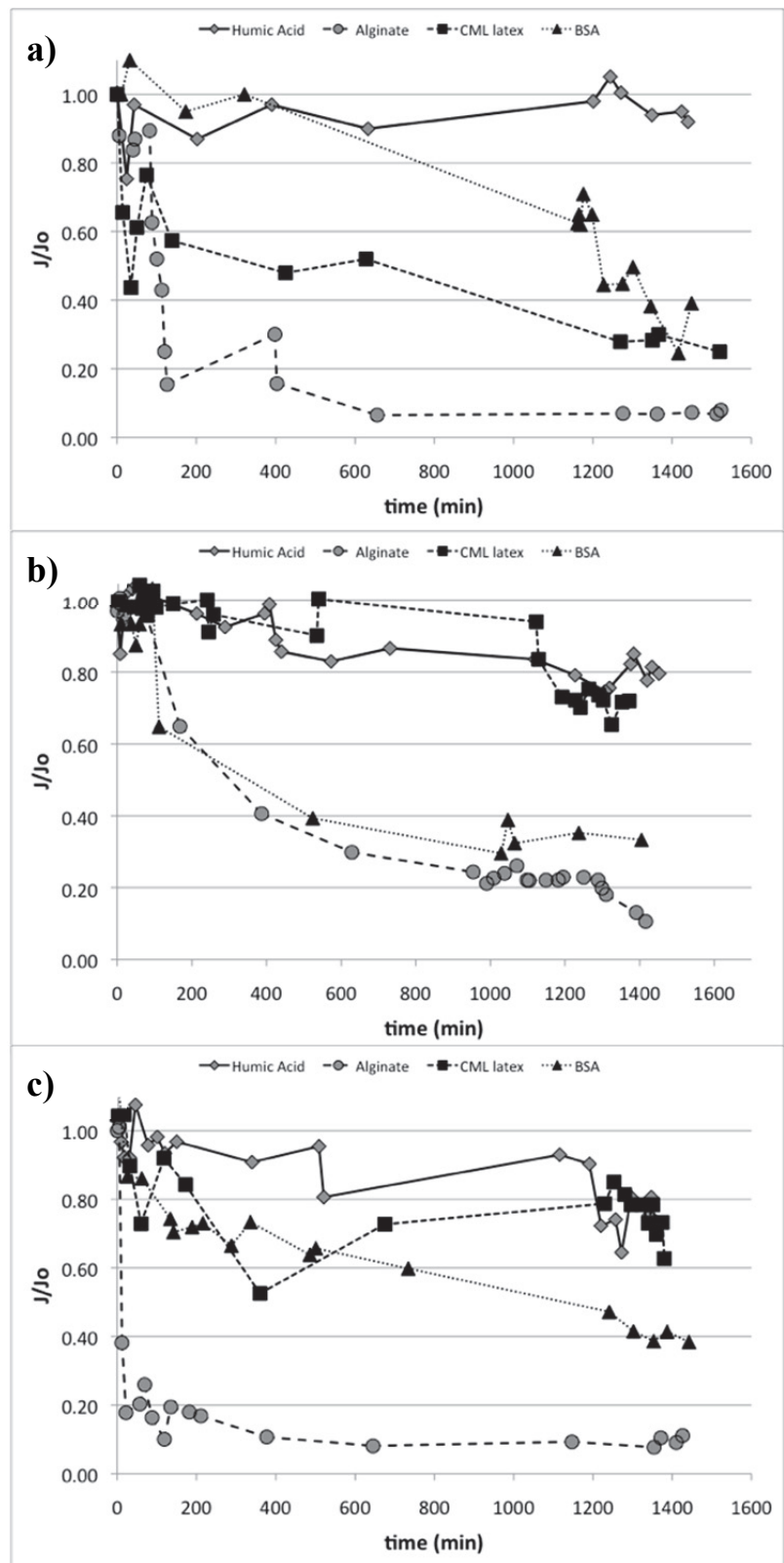


Figure 3.2. Relative flux as a function of time for MD tests of synthetic organic foulants at a concentration of 50 mg/L for anodisc membrane coupons filtering water over 24 h at (a) pH=3, (b) pH=7, and (c) pH=10.

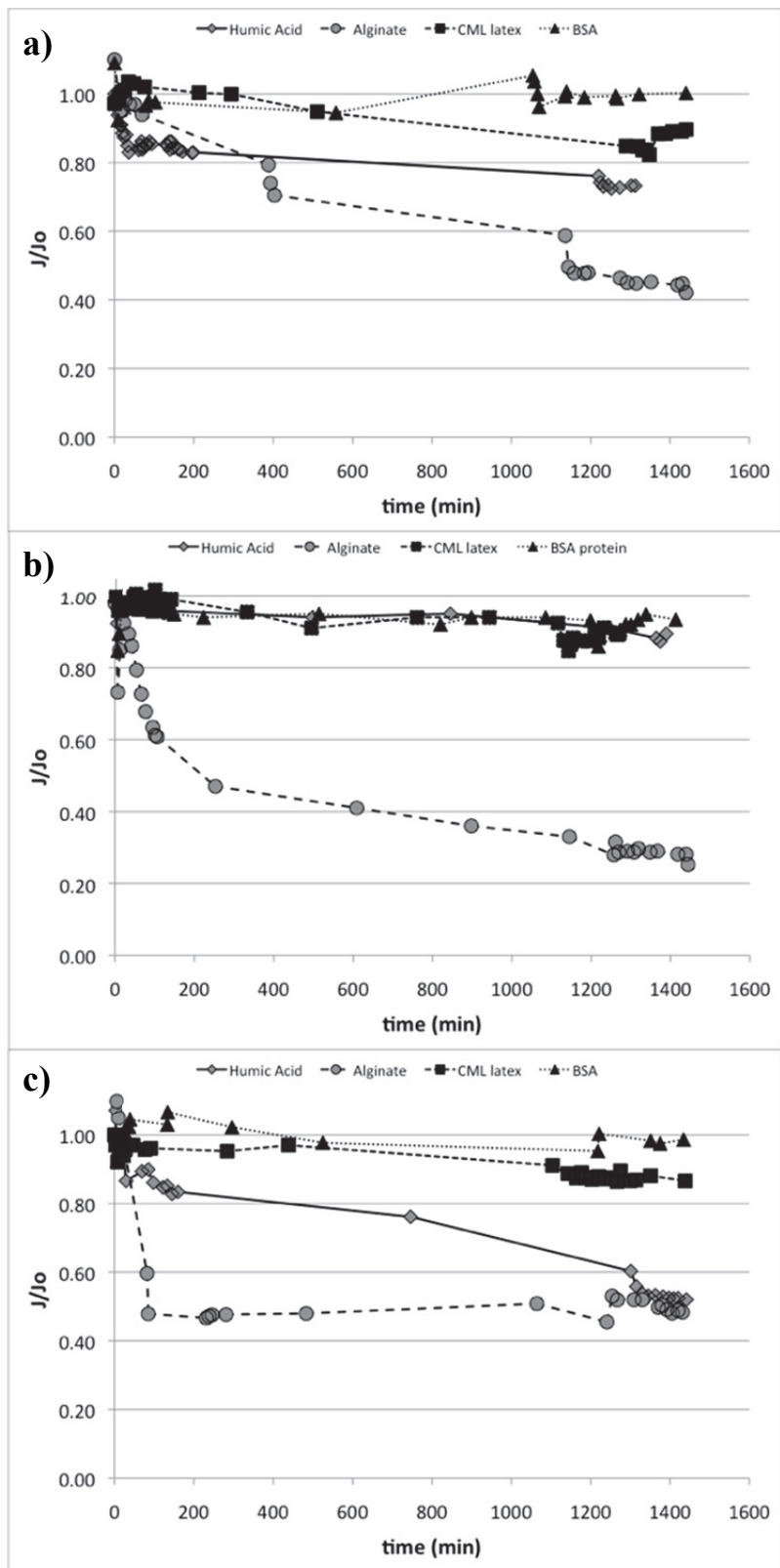


Figure 3.3. Relative flux as a function of time for MD tests of synthetic organic foulants at a concentration of 50 mg/L for TF-200 membrane coupons filtering water over 24 h at (a) pH=3, (b) pH=7, and (c) pH=10.

The data represented in Figures 3.2 and 3.3 provide a significant amount of information about the fouling tests, and at first glance, it is difficult to identify trends that explain the fouling phenomena observed. However, there are some readily available observations. The first is that alginate reduces the membrane flux more than do all other foulants at all conditions for both membranes. This finding suggests that a feed water with a significant concentration of EPS may not be a suitable candidate for MD treatment. The most obvious reason for alginate's greater impact on flux decline is that it is the most hydrophobic foulant, which, because both membranes tested are also highly hydrophobic, greatly increases the probability of deposition on the membrane surface once contact is made. However, SEM images showed the buildup of a foulant layer on all membranes tested, indicating that the structure and properties of the layer are at least as important as the absolute mass of the foulant present on the membrane. Figure 3.4a through f show representative images of various fouled membranes. Although all membranes were imaged, a handful are presented for brevity.

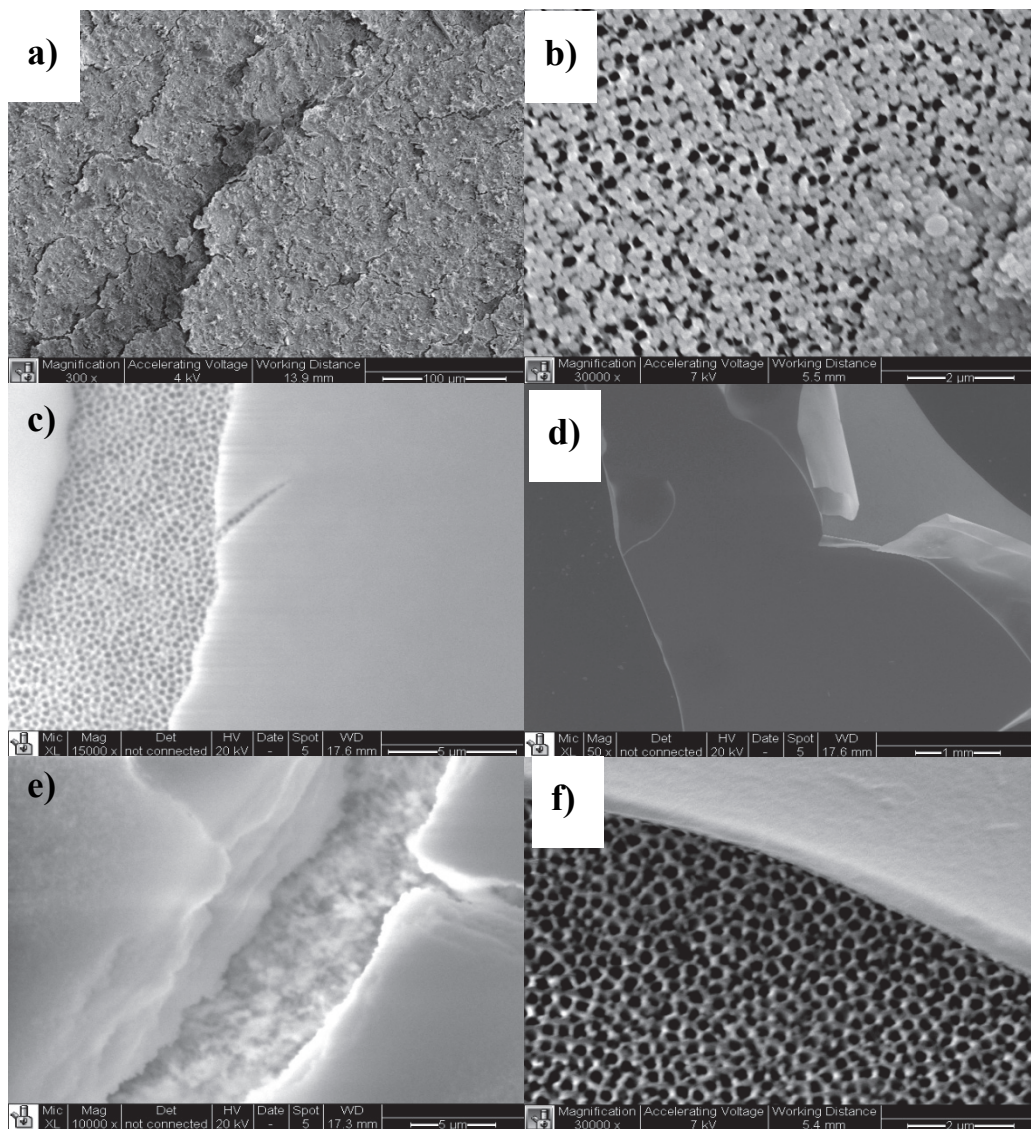


Figure 3.4. Representative SEM images of fouled membranes: (a) TF-200, humic acid, pH=7, (b) anodisc, CML, pH=10, (c) anodisc, alginate, pH=7, (d) TF-200, alginate, pH=7, (e) TF-200, BSA, pH=3, and (f) anodisc, BSA, pH=7.

Although the fouling layer is likely to undergo structural changes during the dehydration process, the images still provide clues as to the different behavior. Figure 3.4c shows the “curling” that was characteristic for all alginate-fouled membranes upon drying. The film formed on the membranes by all the other foulants cracked upon drying, whereas the alginate films seemed almost plastic-like. The foulant layer formed by alginate appears to be a much tighter mesh than that formed by the other foulants, which is more effective at restricting water penetration. In fact, alginate is known to polymerize in the presence of calcium compounds, forming gels and membranes, in many biomedical applications [61]. The sharp drop in flux for both membrane types at pH=10 (Figure 3.2c and 3.3c) suggests that this reaction rate is increased under basic conditions, but this theory was not verified in the literature, where the polymerization reactions took place under neutral conditions. Alternatively, it is possible that the gel structure changes by swelling under different pH conditions [62]. The images could not be used to explain all discrepancies in flux decline. For example, the SEM images of PTFE membranes fouled with humic acid looked very similar at pHs of 7 and 10 (not shown), whereas the flux decline was drastically different for each of these test runs, suggesting that the hydrated structure of each foulant layer exhibits differences that cannot be captured by imaging dried membranes.

Another key trend noted by comparing Figures 3.2 and 3.3 is that for nearly all of the experimental runs (the exceptions being humic acid at pH = 3 and pH = 10), the anodisc membranes exhibit a greater flux decline than do their PTFE counterparts. The average difference between all tests shows that the PFS anodisc membranes exhibit a 29% greater flux decline (and is as large as 60% in a few instances). It is likely that this flux decline is at least partially attributable to the anodisc membranes having smaller pores than do their PTFE counterparts, which increases the rate of flux decline [55]. Previous work comparing the LEP values of the PFS and PTFE membranes showed that, although both manufacturers list a nominal pore size of 200 nm, the PTFE membranes have a significant number of pores greater than this value [63]. However, it cannot be ruled out that the PFS membranes are more prone to fouling because of their surface chemistry. This possibility is so especially in light of the various flux decline behaviors observed for different foulants on each membrane. Tables 3.2 and 3.3 present the average end value of each fouling test and average these values across pH and foulant type. A series of replicate experiments were performed at each pH with one foulant for each membrane to measure the final relative flux values and to compare them with the data presented in Figures 3.2 and 3.3. The largest difference between observed flux values was 0.07, whereas the average was 0.04.

Table 3.2. Final Relative Flux Value for Each Synthetic Fouling Experimental Test, Averaged by Foulant Type and by pH^a

Foulant	Value for:			
	J_{final}/J_0 , pH = 3	J_{final}/J_0 , pH = 7	J_{final}/J_0 , pH = 10	Avg w/SD
Humic acid	0.92	0.80	0.81	0.84 ± 0.07
Alginate	0.07	0.11	0.11	0.10 ± 0.02
CML	0.25	0.72	0.63	0.53 ± 0.35
BSA	0.39	0.33	0.38	0.37 ± 0.03
Avg w/SD	0.41 ± 0.37	0.49 ± 0.33	0.48 ± 0.30	Avg salt rejection ~94% ± 1.2%

^aPFS anodisc tests.

Table 3.3. Final Relative Flux Value for Each Synthetic Fouling Experimental Test, Averaged by Foulant Type and by pH^a

Foulant	Value for:			
	J_{final}/J_0 , pH = 3	J_{final}/J_0 , pH = 7	J_{final}/J_0 , pH = 10	Avg w/SD
Humic acid	0.73	0.93	0.52	0.73 ± 0.21
Alginate	0.42	0.28	0.49	0.40 ± 0.11
CML	0.90	0.89	0.87	0.89 ± 0.02
BSA	1.0	0.93	0.99	0.97 ± 0.04
Avg w/SD	0.76 ± 0.25	0.76 ± 0.32	0.72 ± 0.25	Avg salt rejection >99%

^aTF-200 tests.

Although selectively grouping the endpoint data points of the synthetic fouling tests does not provide insight about the fouling evolution over time, it does allow us to make several important observations about the final flux states of the membranes. First, for both membrane types tested, the pH effect is generally less influential than the type of foulant tested. Overall, averaging the final flux values across pH values does give similar average values but with very high standard deviation. However, when averging the flux values by foulant type, we see that generally there is little change with pH. Although there are exceptions (CML with PFS and humic acid with PTFE), it appears that the dominant interactions between the synthetic organic foulants and the membrane surface that determine the fouling potential are independent of the pH of the feed solution. We also see that membrane type is important in

determining fouling potential and that for the PFS anodisc membrane, the synthetic foulants in order of increasing flux decline are alginate > BSA > CML > humic acid, whereas for the PTFE membrane, they are alginate > humic acid > CML > BSA. It was explained earlier why alginate has such a significant impact on flux decline, but it is not immediately apparent why humic acid and BSA act in a nearly opposite manner for both membrane types. A final important observation is that the TF-200 membranes consistently exhibit superior salt rejection, which is attributed to imperfections in the coating process of the PFS membranes. However, we note that this rejection level did not vary by foulant type or pH. The salt rejection values given in Tables 3.2 and 3.3 were averaged throughout the experiments. Salt rejection was maintained throughout the experiments and was observed to be independent of time, pH, and foulant type. Foulant rejection was measured via total organic carbon samples of the permeate, giving 100% rejection for all foulants, which was expected because the particulate material is not volatile and does not approach the size of salt ions that do cross the membrane.

For the exceptions noted earlier (CML with PFS and humic acid with TF-200), where fouling increases as the pH shifts from 7 to 10, it is immediately unclear why there would be such a drastic change in foulant/membrane affinity. According to Table 3.1, particle size and zeta potential are nearly constant within this pH range, suggesting that the pH change must alter the membrane surface enough to affect its interaction with the foulants. Although it is not possible to explain all the variation observed during the synthetic foulant studies, there are several key observations to take away that may aid in the subsequent wastewater studies. The first is that pH is not expected to have much of an impact on the fouling or rejection observed during operation. In addition, because the water is downstream from an activated sludge tank, the organic content is likely to be dominated by biological matter that resembles BSA and alginate more closely than it resembles humic substances, so we expect that the flux decline will be more pronounced for the PFS membrane than for the TF-200 membrane.

3.7 Synthetic Foulant Effect on LEP

Although measuring and understanding the flux decline provide vital information for operation, another important goal of the foulant studies is to determine the impact of the foulant layer on the membrane pore structure. In particular, we are interested in ascertaining if the presence of the organic foulants impacts the LEP of the membranes, which would impact the long-term operation conditions of the membranes. This task was accomplished by performing LEP tests on fouled membranes, the results of which are given in Figures 3.5 and 3.6.

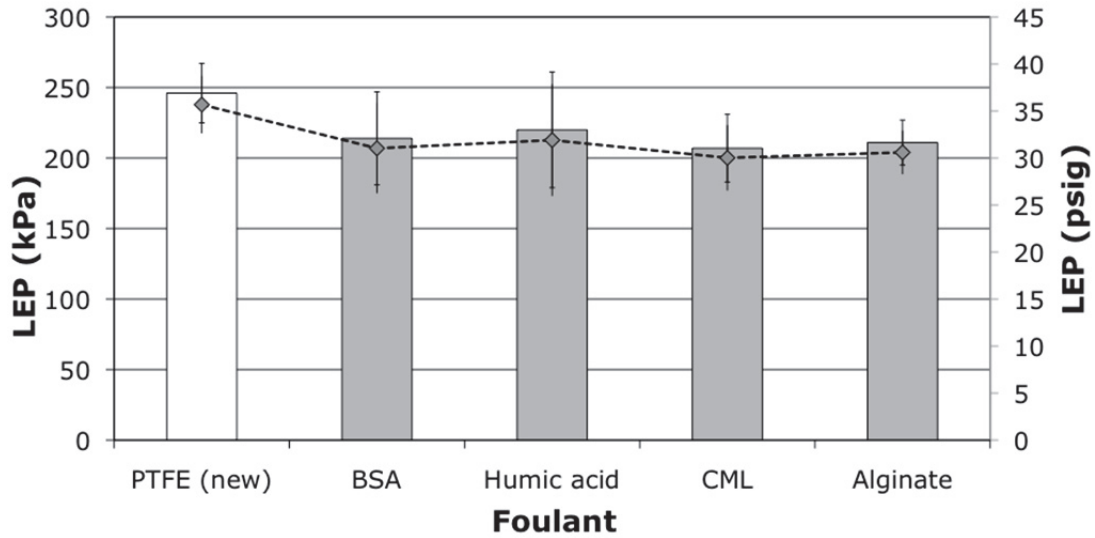


Figure 3.5. LEP results for TF-200 membranes fouled with synthetic foulants averaged for all three pH values. Columns are in kilopascal pressure units, and data points are in pounds per square inch gauge.

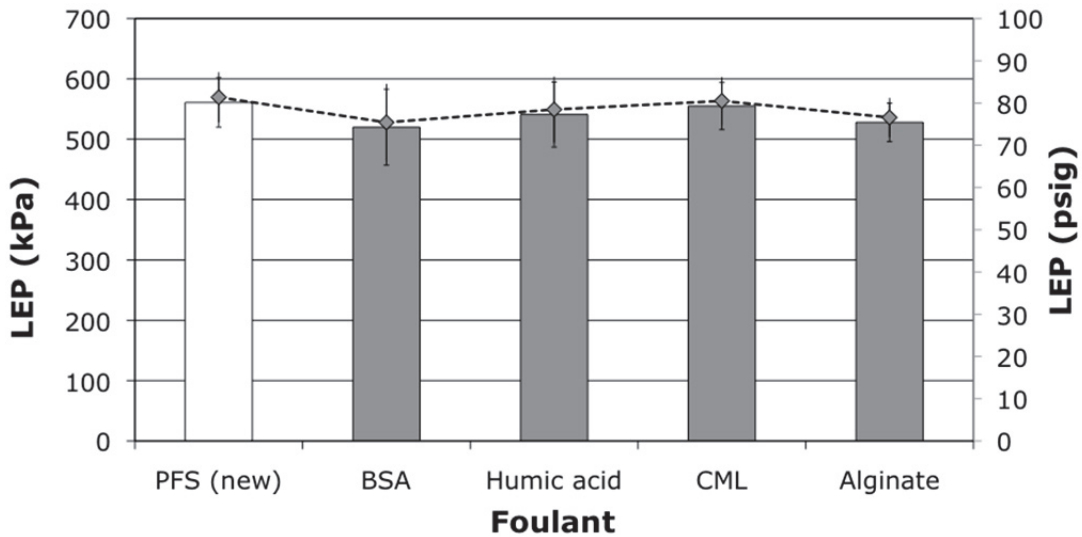


Figure 3.6. LEP results for PFS anodisc membranes fouled with synthetic foulants averaged for all three pH values. Columns are in kilopascal pressure units, and data points are in pounds per square inch gauge.

The figures show a slight decline in the average LEP for all membranes exposed to fouling tests but also show this decline is within the standard deviation of the clean membrane LEP tests. We can conclude that the effect of the foulant layer on the membrane surface is negligible and that, at least initially, the fouling layer will not affect the operating pressure during MD. However, it is noteworthy that the average flux decline was below the clean membrane value, and long-term studies are warranted to determine if the LEP decreases over the operational lifetime of a membrane.

3.8 Membrane Distillation of 2^o Clarified Effluent

The final phase of this project was to investigate membrane performance during MD treatment of secondary clarified wastewater from the North Durham Water Reclamation Facility. The facility has a 20-million-gallon-per-day capacity, and the facility includes tertiary treatment. The treatment train includes bar screens/prefilters, a primary settling tank, activated sludge aeration tanks, secondary clarification, and final filtration, as well as chlorine and UV disinfection. Table 3.4 summarizes the National Pollutant Discharge Elimination System (NPDES) permit limits and the average, high, and low effluent values.

Table 3.4. NPDES Permit Limits and Average Monthly Discharge Values for the North Durham Water Reclamation Facility

Parameter	Flow	MGD	TSS	mg/L	Fecal Coliform, No./mL	Conductivity, mohm/cm
Avg	8.23		1.8		37	448.94
Min	6.49		0.43		6	382.71
Max	11.23		4.25		134	527.00
Limit	20		30		200	N/A

3.9 Wastewater Fouling Tests

The MD fouling tests were conducted in a manner similar to that of the synthetic fouling experiments. The baseline initial water flux was established by using DI water prior to filtration of the secondary clarified wastewater. The temperature gradient and flow rates used were identical to those selected earlier. Figure 3.7 displays the flux decline results for MD tests in which both PFS and TF-200 membranes were used.

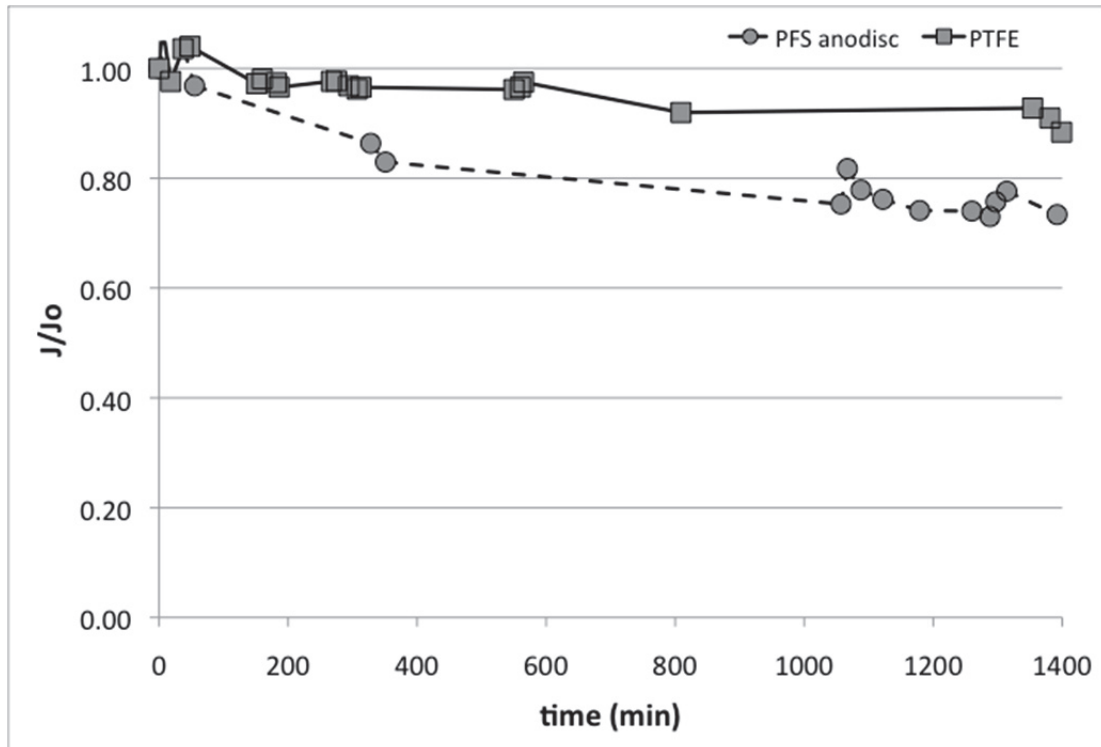


Figure 3.7. Relative flux as a function of time for TF-200 and PFS membranes during MD of 2° clarified effluent from the North Durham Water Reclamation Facility.

Figure 3.7 shows that, as expected, the PFS membrane exhibits a greater flux decline than does the TF-200 membrane. The difference in the final flux after 24 h is a 15% greater drop in water flux for the PFS anodisc, which is lower than the overall average difference observed for the synthetic foulants. Including these new data into the fouling potentials observed for the synthetic foulants shows that, for PFS membranes the order of increasing flux decline is alginate > BSA > CML > 2° WW > humic acid, whereas, for the TF-200 membrane, it is alginate > humic acid > CML ~ 2° WW > BSA, which shows that the water flux decline caused by the wastewater is relatively low for both membrane materials when compared with that for the synthetic fouling solutions. Of key interest to utilities that might consider MD technology as a tertiary treatment alternative will be the contaminant effluent values. An analytical summary is given in Table 3.5.

Table 3.5. Measured Values of Key Discharge Parameters for Secondary Clarified Wastewater Filtered via MD with Both PFS and PTFE Membranes

Substance or Limit	Value for:		
	TSS (mg/L) ^a	Fecal Coliform (No./mL)	Conductivity (μmohm/cm)
Wastewater	21.2	57	514.6 ± 13.5
PTFE effluent	<0.01	0	12.9 ± 3.8
PFS effluent	<0.01	0	73.6 ± 11.1
NPDES limit	30	200	N/A

^aTSS, total suspended solids. MD effluent values are measured from overall effluent and adjusted for dilution effect of DI water.

The results show that MD technology easily exceeds the NPDES permit limits and provides discharge water of extremely high quality. This finding is expected, because the primary contaminants in the wastewater are organic material and salts are readily separated via the vapor separation mechanism of MD. Larger contaminants like particles/bacteria/fecal coliform are already rejected by using MF membranes under pressure operation, so they are expected to be easily rejected in the absence of high pressures such as MD, where a temperature gradient is applied across these membranes. These results show that the risk associated with exploring MD technology does not lie in a reduction in effluent quality, which may reduce the barrier for implementation for utilities seeking to explore energy-saving water treatment methods.

3.10 Membrane-Cleaning Experiments

Another important goal of this project was to determine the effectiveness of cleaning methods on the membrane water flux recovery during MD. These cleaning experiments provide information on the reversible versus irreversible nature of the foulant layer and are useful in developing effective cleaning strategies for the membranes during operation. The original experimental proposal included plans to investigate air back-pulsing as a cleaning method; however, preliminary tests showed that this method did not effectively remove the foulant layer; therefore, solution scouring of the membrane's surface was tested. The following cleaning solutions were chosen: deionized (DI) water, a 100-ppm solution of NaOCl at pH = 7, and a 100-ppm solution at pH = 10. The cleaning solution was not tested at pH = 3 to prevent the possible formation of chlorine gas under acidic conditions. Sodium hypochlorite was selected because it is a proven cleaning agent for organic/biological material and because it poses no risk for effluent contamination. DI water was selected to provide a comparison using a low-cost alternative. Cleaning results for both the PFS and TF-200 membranes are provided in Figures 3.8 and 3.9.

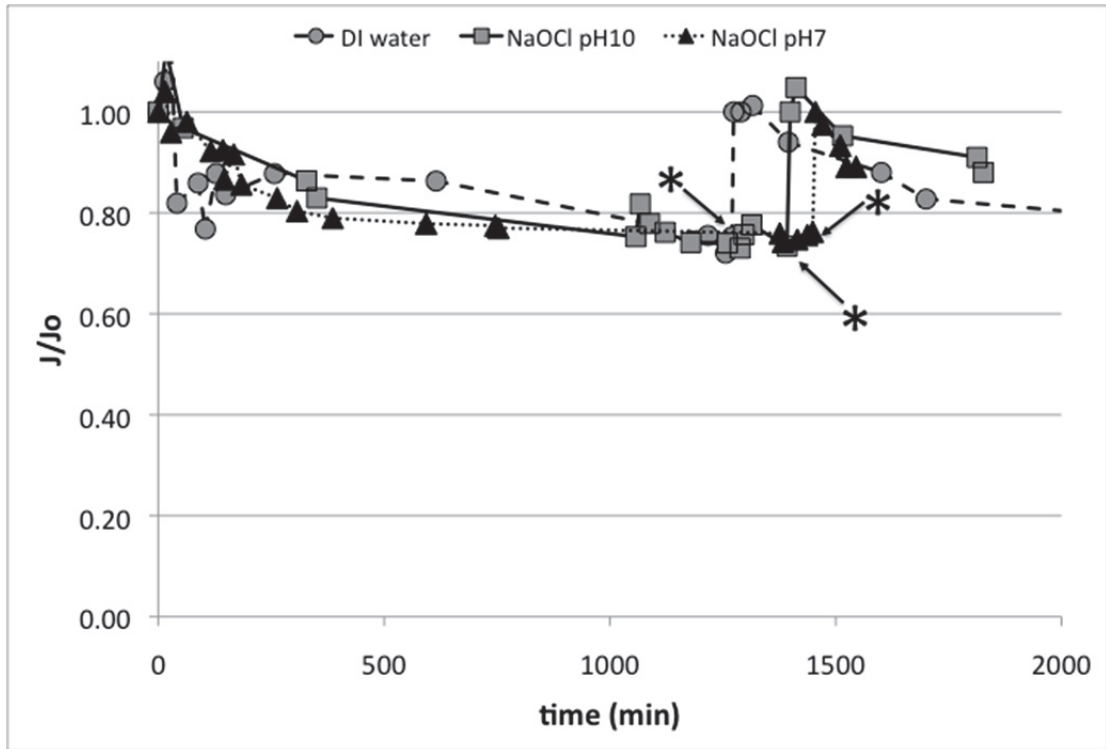


Figure 3.8. Membrane distillation of secondary clarified wastewater incorporating one of three cleaning solutions. PFS anodisc membranes. The * denotes the time of membrane cleaning.

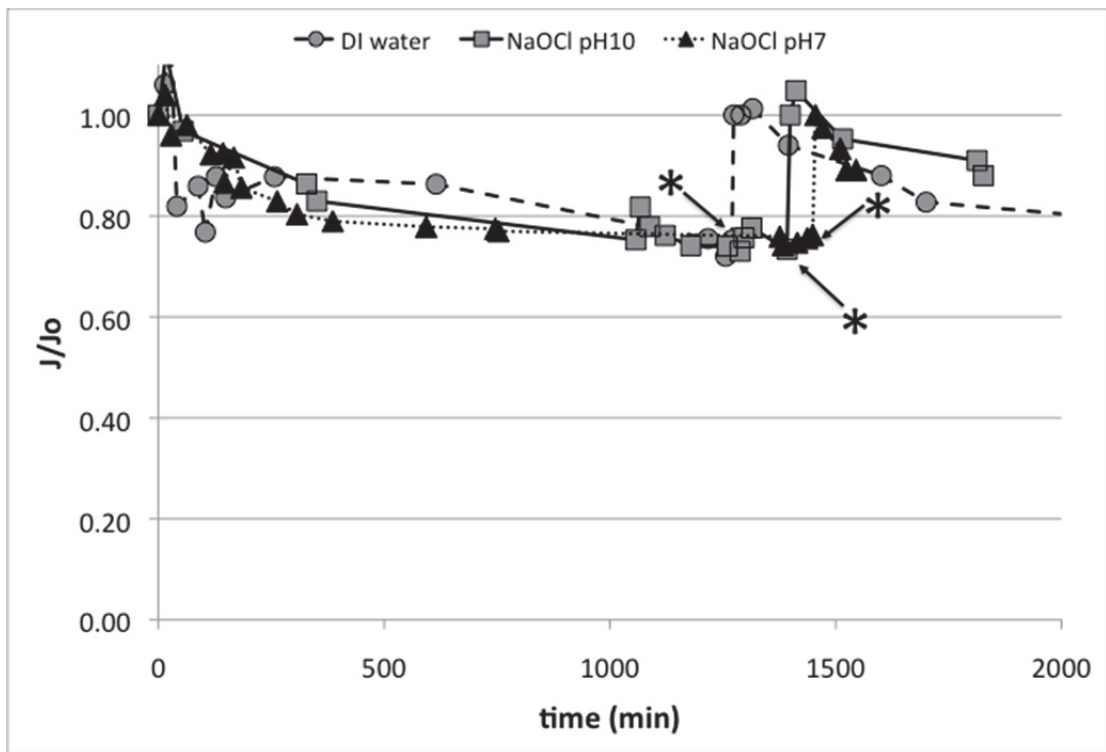


Figure 3.9. Membrane distillation of secondary clarified wastewater incorporating one of three cleaning solutions. TF-200 membranes. The * denotes the time of membrane cleaning.

The cleaning tests shown in Figures 3.8 and 3.9 proved that all cleaning solutions resulted in a virtually complete water flux recovery. In addition, single-LEP measurements on membranes after they were cleaned by each of the solutions resulted in entry pressure values within the standard deviation of new membranes (250, 235, and 241 for TF-200 and 529, 545, and 536 for PFS anodisc membranes after exposure to sodium hypochlorite and pH = 7, pH = 10, and plain DI water, respectively). Although these are promising results for MD technology, further research using different feed waters, longer periods, and other membranes are required to fully assess the performance of MD under a wider range of conditions. For the PFS membrane, both the DI water and sodium hypochlorite at pH = 10 solutions resulted in 100% recovery; whereas the sodium hypochlorite at pH = 7 resulted in 97% recovery, which is within the measurement error for the membrane module. For the TF-200 membrane, all three cleaning solutions yielded a 99% flux recovery. We can deduce that, because the system is operated under low pressures (5–6 psig) in comparison with those used in pressure-driven membrane processes, the foulant film that forms on the membrane surface is therefore loosely packed and easily removed. The fact that plain DI water performed on par with both the chemical cleaning solutions represents a potentially significant area for saving money for MD technology. Both the PFS and TF-200 membranes were imaged via SEM before and after cleaning; representative images are presented in Figure 3.10.

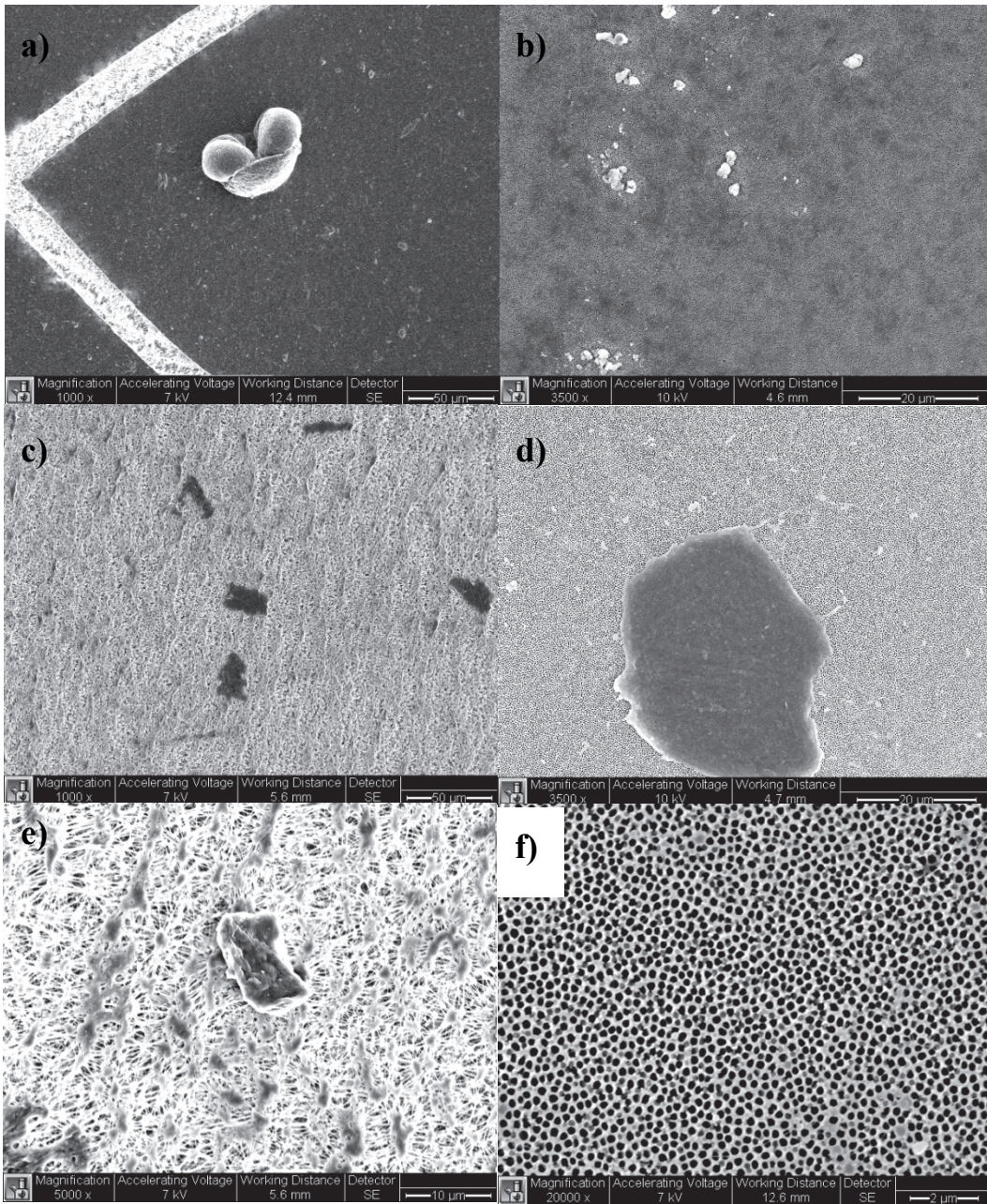


Figure 3.10. Representative images of membranes after filtering wastewater via MD before and after cleaning: (a) fouled TF-200 membrane, (b) fouled PFS membrane, (c) TF-200 membrane cleaned with NaOCl at pH=7, (d) PFS membrane cleaned with NaOCl at pH=10, (e) TF-200 membrane cleaned with NaOCl at pH=10, and (f) PFS membrane cleaned with DI water.

Figure 3.10a and 3.10b shows the fouling layer on both the polymeric and ceramic membranes. The fouling layer appears to be uniformly spread on the TF-200 membrane, with cracks on the layer evident from drying, whereas for the PFS membrane, the layer has a blotchy quality. Figure 3.10a also provides a close-up of an organism deposited on the membrane surface. Figure 3.10c and d show that, for both membranes, the cleaning was not 100% effective, as deposits that were not removed during cleaning remain. This finding was evident for all cleaning methods used. Figure 3.11e and 3.11f provides a close-up view of the membrane surface and shows that areas that were scoured appear to have been fully restored to their pre-fouled state. If this evidence is combined with the flux recovery graphs in Figures

3.9 and 3.10, we can surmise that the cleaning methods are highly effective in restoring water flux but that long-term membrane tests are needed to determine if/when the foulant remnants begin to contribute to irreversible flux decline.

3.11 Wastewater Fouling Effect on LEP

As done in the synthetic foulant studies, the LEP of wastewater-fouled membranes was measured to determine if the foulant layer played a role in reducing the entry pressure by altering the pore structure. The results are presented in Figure 3.11.

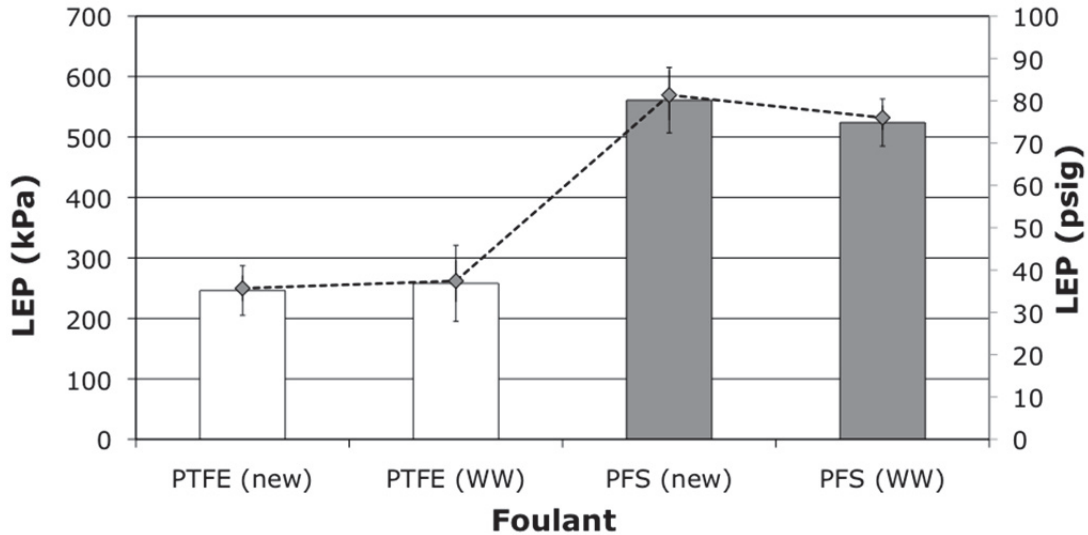


Figure 3.11. LEP results for PFS anodisc and TF-200 membranes fouled with secondary clarified effluent from the North Durham Water Reclamation Facility. Wastewater results averaged for all two measurements.

Although the figure from the LEP tests shows a slight increase in LEP for the TF-200 membranes and a slight decrease for the PFS membranes, both results are within the standard deviation, and we can conclude that there is no change in the entry pressure. This is as expected from the earlier results of the synthetic foulant studies and further confirms the conclusion that the foulants have not entered the pore matrix of the membranes but rather remained on the surface.

The data presented in this chapter show that the LEP values of both the PFS anodisc and TF-200 membranes are maintained well within operational limits required to prevent pore flooding after exposure to the four synthetic foulants and to wastewater as well as after cleaning. Alginate, a surrogate for EPS, was shown to cause the most fouling of the synthetic foulants tested. Measured flux decline showed that the TF-200 membranes displayed overall lower flux decline over time for all foulants and wastewater experiments. Membrane-cleaning experiments demonstrated that DI water performed on par with sodium hypochlorite solutions at pHs of 7 and 10, yielding flux recoveries after cleaning between 97 and 100%.

Chapter 4

Conclusions and Final Recommendations

The work completed in this project provides information in several key areas that is important for advancing our knowledge of MD as a water reuse technology option. The following conclusions can be made from the information obtained and experiments performed throughout this project:

- The surface chemistry of ceramic membranes can be successfully modified to yield a hydrophobic surface suitable for use in MD.
- The hydrophobic surfaces of both the modified ceramic and PTFE membrane are resistant to exposure to high concentrations of chlorine, with the PFS anodisc shown to exhibit the greatest resistance to loss of hydrophobicity. However, both membranes can be said to exhibit properties that would allow for high concentrations of chlorine for the prevention/removal of biofouling should that be required in future MD operation.
- The modified ceramic membranes provide a water flux approximately 45% lower than that of PTFE TF-200 membranes during MD operation. This lower flux is attributed primarily to a combination in the differences between the thermal conductivity and porosity of the membranes.
- The uniform pore size and structure of the ceramic membranes provide a higher LEP, which makes it more viable than PTFE for MD applications where high-pressure or low-surface-tension feedwaters are present.
- With the exception of humic acid, the PTFE membrane exhibited a greater resistance to flux decline when exposed to solutions containing organic foulants, including secondary clarified wastewater.
- The foulant layers had no significant effect on the LEP of either the PTFE or PFS anodisc membranes. This finding suggests that the foulants did not enter the pore matrix of the membranes, which means that membrane rejection properties are not likely to degrade over time.
- The water quality of the treated effluent was exceedingly high and would easily meet permitting standards. There is a low risk of reduced water quality for the implementation of a thermally driven MD process.
- Complete water flux recovery of membranes fouled after treating wastewater was achieved by using either sodium hypochlorite solutions or DI water. This finding represents an area of potential cost savings, because reducing or eliminating the need for chemicals during membrane cleaning would lower operating costs.

In addition to the questions answered by the results presented in this work, additional areas have been identified that require further investigation. Foremost of these is the performance

of water flux and contaminant rejection over a period longer than 24 h. Although it is an extremely promising development that virtually complete flux recovery was achieved with only water as the cleaning agent, it is important to identify if and when fouling becomes irreversible, which has implications on both operational strategies and membrane lifetime. This information can be obtained only by exposing these membranes to continuous operation for weeks or months so that changes in performance over the long term can be assessed. This feat would be best accomplished by an extended investigation, preferably on the pilot scale, which could be used to identify both advantages and problems that might arise when one is implementing this new technology.

Although the small lab scale of the experiments here is beyond the scope of detailed economic analysis, there are several important generalizations to be made from the data gathered throughout this project. Ceramic membranes tend to be more expensive than polymeric membranes; their use is incentivized when operational conditions are such that either their longer life span (and therefore fewer module replacements) offsets the higher initial capital investment or when temperatures or chemical cleaning methods are required that would destroy a polymeric counterpart. Because both membranes investigated showed high flux recovery, though maintaining properties necessary for continued DCMD operation, the results here do not suggest an advantage for one membrane over the other. The specific requirements of a given water treatment scenario will dictate whether the longer life span and increased durability of a ceramic membrane make it the more economic alternative.

Finally, the findings in this report are based on data gathered on the lab scale and over shorter periods than those that would be required on larger scales. Continued experimentation on larger scales is necessary to continue to advance the state of the current knowledge of this technology and to inform stakeholders how to make the most economical decisions. MD is an attractive technology for water reuse when there is available thermal energy to serve as the separation driving force, with the strong possibility of cost savings to users, and the results here indicate that continued research on a larger scale is warranted. Future efforts should be made with partners who have a readily available heat source so that pilot modules can be integrated into existing process configurations to continue the vetting of this technology.

References

1. Meindersma, G. W.; Guijt, C. M.; Haan, A. B. Desalination and water recycling by air gap membrane distillation. *Desalination* **2006**, *187*, 291–301.
2. Song, L.; et al. Performance limitation of the full-scale reverse osmosis process. *J. Membr. Sci.* **2003**, *214*, 239–244.
3. van der Bruggen, B.; Lejon, L.; Vandecasteele, C. Reuse, treatment, and discharge of the concentrate of pressure driven membrane processes. *Environ. Sci. Technol.* **2003**, *37*, 3733–3738.
4. Burgoyne, A.; Vahdati, M. M. Direct contact membrane distillation—review. *Sep. Sci. Technol.* **2000**, *35*, 1257–1284.
5. Lior, A. M. Membrane-distillation desalination: status and potential. *Desalination* **2005**, *171*, 20.
6. Cath, T. Y.; Adams, V. D.; Childress, A. E. Experimental study of desalination using direct contact membrane distillation: a new approach to flux enhancement. *J. Membr. Sci.* **2004**, *228*, 5–16.
7. Martinez-Diez, L.; Florido-Diez, F. J.; Vazquez-Gonzalez, M. I. Study of polarization phenomena in membrane distillation of aqueous salt solutions. *Sep. Sci. Technol.* **2000**, *35*, 1485–1501.
8. Mulder, M. H. V. *Basic Principles of Membrane Technology*, 2nd ed.; Kluwer Academic Publishers: Dordrecht, The Netherlands, 1997.
9. Schofield, R. W.; Fane, A. G.; Fell, C. D. J. Factors affecting flux in membrane distillation. *Desalination* **1990**, *77*, 279–294.
10. Gryta, M.; Tomaszewska, M. Heat transport in the membrane distillation process. *J. Membr. Sci.* **1998**, *144*, 211–222.
11. Phattaranawik, J.; Jiratananon, R.; Fane, A. G. Heat transport and membrane distillation coefficient in direct contact membrane distillation. *J. Membr. Sci.* **2003**, *212*, 177–193.
12. Lawson, K. W.; Lloyd, D. R. Membrane distillation. *J. Membr. Sci.* **1997**, *124*, 1–25.
13. Song, L.; et al. Direct contact membrane distillation-based desalination: novel membranes, devices, larger-scale studies, and a model. *Ind. Eng. Chem. Res.* **2007**, *46*, 2307–2323.
14. Gryta, M.; Tomaszewska, M. Heat transport in the membrane distillation process. *J. Membr. Sci.* **1998**, *144*, 211–222.
15. Termpiyakul, P.; Jiratananon, R.; Srisurichan, S. Heat and mass transfer characteristics of a direct contact membrane distillation process for desalination. *Desalination* **2005**, *177*, 133–141.
16. Kays, W. M.; Lunberg, R. E.; Reynolds, W. C. Heat Transfer with Laminar Flow in Concentric Annuli with Constant and Variable Wall Temperature and Heat Flux. <http://ntrs.larc.nasa.gov/search.jsp?R=19620000972&q=Ns%3DPublication-Date%7C0%26N%3D4294964889> (accessed March 2012), 1961, p 212.

17. Phattaranawik, J.; Jiratananon, R.; Fane, A. G. Heat transport and membrane distillation coefficients in direct contact membrane distillation. *J. Membr. Sci.* **2003**, *212*, 177–193.
18. Hsu, S. T.; Cheng, K. T.; Chiou, J. S. Seawater desalination by direct contact membrane distillation. *Desalination* **2002**, *143*, 279–287.
19. Schofield, R. W.; Fane, A. G.; Fell, C. D. J. Gas and vapor transport through microporous membrane. I. Knudsen-Poiseuille transition. *J. Membr. Sci.* **1990**, *53*, 159–171.
20. *Desalination Markets 2007: A Global Industry Forecast*; Media Analytics Ltd.: Oxford, England, 2006.
21. Criscuoli, A.; Drioli, E. Energetic and exergetic analysis of an integrated membrane desalination system. *Desalination* **1999**, *124*, 243–249.
22. Yun, Y.; et al. Direct contact membrane distillation mechanism for high concentration NaCl solutions. *Desalination* **2006**, *188*, 251–262.
23. Gryta, M. Long-term performance of membrane distillation process. *J. Membr. Sci.* **2005**, *265*, 153–159.
24. Song, L.; et al. Pilot plant studies of novel membranes and devices for direct contact membrane distillation-based desalination. *J. Membr. Sci.* **2008**, *323*, 257–270.
25. Cath, T. Y.; Adams, V. D.; Childress, A. E. Experimental study of desalination using direct contact membrane distillation: a new approach to flux enhancement. *J. Membr. Sci.* **2004**, *228*, 5–16.
26. Xu, Y.; Zhu, B.-K.; Xu, Y.-Y. Pilot test of vacuum membrane distillation for desalination on a ship. *Desalination* **2006**, *189*, 165–169.
27. Martinez, L.; Rodriguez-Maroto, J. M. Characterization of membrane distillation modules and analysis of mass flux enhancement by channel spacers. *J. Membr. Sci.* **2006**, *274*, 123–137.
28. Srisurichan, S.; Jiratananon, R.; Fane, A. G. Mass transfer mechanisms and transport resistances in direct contact membrane distillation process. *J. Membr. Sci.* **2006**, *277*, 186–194.
29. Izquierdo-Gil, M. A.; Fernández-Pineda, C.; Lorenz, M. G. Flow-rate influence on direct contact membrane distillation experiments: different empirical correlations for Nusselt number. *J. Membr. Sci.* **2008**, *321*, 356–363.
30. Benfer, A.; et al. Development and characterization of ceramic nanofiltration membranes. *Sep. Purif. Technol.* **2001**, *22–23*, 231–237.
31. Cortalezzi, M. M.; et al. Characteristics of ceramic membranes derived from alumoxane nanoparticles. *J. Membr. Sci.* **2002**, *205*, 33–43.
32. Cortalezzi, M. M.; et al. Ceramic membranes derived from ferroxane nanoparticles: a new route for the fabrication of iron oxide ultrafiltration membranes. *J. Membr. Sci.* **2003**, *227*, 207–217.
33. Leger, C.; Lira, H. D. L.; Paterson, R. Preparation and properties of surface modified ceramic membranes. Part II. Gas and liquid permeabilities of 5 nm alumina membranes modified by a monolayer of bound polydimethylsiloxane (PDMS) silicone oil. *J. Membr. Sci.* **1996**, *120*, 135–146.

34. Picard, C.; et al. Grafting of ceramic membranes by fluorinated silanes: hydrophobic features. *Sep. Purif. Technol.* **2001**, *25*, 65–69.
35. Krajewski, S. R.; et al. Application of fluoroalkylsilanes (FAS) grafted ceramic membranes in membrane distillation process of NaCl solutions. *J. Membr. Sci.* **2006**, *281*, 253–259.
36. Sah, A.; et al. Hydrophobic modification of γ -alumina membranes with organochlorosilanes. *J. Membr. Sci.* **2004**, *243*, 125–132.
37. Picard, C.; et al. Characterisation of hydrophilic ceramic membranes modified by fluoroalkylsilanes into hydrophobic membranes. *Solid State Sci.* **2004**, *6*, 605–612.
38. Koonaphapdeelert, S.; Li, K. Preparation and characterization of hydrophobic ceramic hollow fibre membrane. *J. Membr. Sci.* **2007**, *291*, 70–76.
39. Leger, C.; Lira, H. D. L.; Paterson, R. Preparation and properties of surface modified ceramic membranes. Part III. Gas permeation of 5 nm alumina membranes modified by trichloro-octadecylsilane. *J. Membr. Sci.* **1996**, *120*, 187–195.
40. Dafinov, A.; Garcia-Valls, R.; Font, J. Modification of ceramic membranes by alcohol adsorption. *J. Membr. Sci.* **2002**, *196*, 69–77.
41. El-Bourawi, M. S.; et al. A framework for better understanding membrane distillation separation process. *J. Membr. Sci.* **2006**, *285*, 4–29.
42. van Oss, C. J. *Interfacial Forces in Aqueous Media*; New York, NY: Marcel Dekker, Inc., 1994.
43. Garcia-Payo, M. C.; Izquierdo-Gil, M. A.; Fernandez-Pineda, C. Wetting study of hydrophobic membranes via liquid entry pressure measurements with aqueous alcohol solutions. *J. Colloid Interface Sci.* **2000**, *230*, 12.
44. Brehant, A.; Bonnelye, V.; Perez, M. Comparison of MF/UF pretreatment with conventional filtration prior to RO membranes for surface water desalination. *Desalination* **2002**, *1–3*, 353–360.
45. Khayet, M.; Godino, M. P.; Mengual, J. I. Thermal boundary layers in sweeping gas membrane distillation processes. *AIChE J.* **2002**, *48*, 1488–1497.
46. Costa, A. R.; de Pinho, M. N.; Elimelech, M. Mechanisms of colloidal natural organic matter in fouling in ultrafiltration. *J. Membr. Sci.* **2006**, *281*, 716–725.
47. Yuan, W.; Kocic, A.; Zydney, A. L. Analysis of humic acid fouling during microfiltration using a pore blockage-cake filtration model. *J. Membr. Sci.* **2002**, *198*, 51–62.
48. Taniguchi, M.; Kilduff, J. E.; Belfort, G. Modes of natural organic matter fouling during ultrafiltration. *Environ. Sci. Technol.* **2003**, *37*, 1676–1683.
49. Jarusutthirak, C.; Amy, G.; Croue, J. P. Fouling characteristics of wastewater effluent organic matter (EfOM) isolates on NF and UF membranes. *Desalination* **2002**, *145*, 247–255.
50. Khayet, M.; Velazquez, A.; Mengual, J. I. Direct contact membrane distillation of humic acid solutions. *J. Membr. Sci.* **2004**, *240*, 123–128.
51. Khayet, M.; Mengual, J. I. Effect of salt concentration during the treatment of humic acid solutions by membrane distillation. *Desalination* **2004**, *168*, 373–381.

52. Srisurichan, S.; Jiratananon, R.; Fane, A. G. Humic acid fouling in the membrane distillation process. *Desalination* **2005**, *174*, 63–72.
53. Gryta, M. Fouling in direct contact membrane distillation process. *J. Membr. Sci.* **2008**, *325*, 383–394.
54. Gryta, M. Effect of iron oxides scaling on the MD process performance. *Desalination* **2007**, *216*, 88–102.
55. Gryta, M. Alkaline scaling in the membrane distillation process. *Desalination* **2008**, *228*, 128–134.
56. He, F.; Sirkar, K. K.; Gilron, J. Effects of antiscalants to mitigate membrane scaling by direct contact membrane distillation. *J. Membr. Sci.* **2009**, *345*, 53–58.
57. Gryta, M.; et al. Membrane distillation of NaCl solution containing natural organic matter. *J. Membr. Sci.* **2001**, *181*, 279–287.
58. Buffle, J.; Deladoey, P.; Haerdi, W. The use of ultrafiltration for the separation and fractionation of organic ligands in freshwaters. *Anal. Chim. Acta* **1978**, *101*, 339–357.
59. Jucker, C.; Clark, M. M. Adsorption of aquatic humic substances on hydrophobic ultrafiltration membranes. *J. Membr. Sci.* **1994**, *97*, 37–52.
60. Hong, S.; Elimelech, M. Chemical and physical aspects of natural organic matter (NOM) fouling of nanofiltration membranes. *J. Membr. Sci.* **1997**, *132*, 159–181.
61. Khayet, M.; Velazquez, A.; Mengual, J. I. Direct contact membrane distillation of humic acid solutions. *J. Membr. Sci.* **2004**, *240*, 123–128.
62. Ye, Y.; et al. Fouling mechanisms of alginate solutions as model extracellular polymeric substances. *Desalination* **2005**, *175*, 7–20.
63. Hodgson, P. H.; et al. Cake resistance and solute rejection in bacterial microfiltration: the role of extracellular matrix. *J. Membr. Sci.* **1993**, *79*, 35–53.
64. McDowell, R. H. *Properties of Alginates*; Alginate Industries, Ltd: London, 1977.
65. Ortiz de Zárate, J. M.; Rincón, C.; Mengual, J. I. Concentration of bovine serum albumin aqueous solutions by membrane distillation. *Sep. Sci. Technol.* **1998**, *33*, 283–296.
66. UN Department of Technical Cooperation and Development. The Use of Non-Conventional Water Resources in Developing Countries; United Nations Natural Resources/Water Series No. 14, United Nations Development Programme Report No. ST/ESA/149; United Nations: New York, NY, 1985.
67. Blandino, A.; Macias, M.; Cantero, D. Formation of calcium alginate gel capsules: influence of sodium alginate and CaCl₂ concentration on gelation kinetics. *J. Biosci. Bioeng.* **1999**, *88*, 686–689.
68. Yuk, S. H.; Cho, S. H.; Lee, H. B. Electric current-sensitive drug delivery systems using sodium alginate/polyacrylic acid composites. *Pharm. Res.* **1992**, *9*, 955–957.
69. Hendren, Z.; Brant, J.; Wiesner, M. Surface modification of nanostructured ceramic membranes for direct contact membrane distillation. *J. Membr. Sci.* **2009**, *331*, 1–10.

Advancing the Science of Water Reuse and Desalination



1199 North Fairfax Street, Suite 410

Alexandria, VA 22314 USA

(703) 548-0880

Fax (703) 548-5085

E-mail: Foundation@WaterReuse.org

www.WaterReuse.org/Foundation